

# Hyperspectral Unmixing Network Inspired by Unfolding an Optimization Problem

Chao Zhou

**Abstract**—The hyperspectral image (HSI) unmixing task is essentially an inverse problem, which is commonly solved by optimization algorithms under a predefined (non-)linear mixture model. Although these optimization algorithms show impressive performance, they are very computational demanding as they often rely on an iterative updating scheme. Recently, the rise of neural networks has inspired lots of learning based algorithms in unmixing literature. However, most of them lack of interpretability and require a large training dataset. One natural question then arises: can one leverage the model based algorithm and learning based algorithm to achieve interpretable and fast algorithm for HSI unmixing problem? In this paper, we propose two novel network architectures, named U-ADMM-AENet and U-ADMM-BUNet, for abundance estimation and blind unmixing respectively, by combining the conventional optimization-model based unmixing method and the rising learning based unmixing method. We first consider a linear mixture model with sparsity constraint, then we unfold Alternating Direction Method of Multipliers (ADMM) algorithm to construct the unmixing network structures. We also show that the unfolded structures can find corresponding interpretations in machine learning literature, which further demonstrates the effectiveness of proposed methods. Benefit from the interpretation, the proposed networks can be initialized by incorporating prior information about the HSI data. Different from traditional unfolding networks, we propose a new training strategy for proposed networks to better fit in the HSI applications. Extensive experiments show that the proposed methods can achieve much faster convergence and competitive performance even with very small size of training data, when compared with state-of-art algorithms.

**Index Terms**—Hyperspectral unmixing, unfolding network, ADMM.

## I. INTRODUCTION

**H**YPERSPECTRAL (HSI) unmixing problem has been developed in Remote Sensing domain for quite a longer period of time. Electro-optical remote sensing has been exploited for the acquisition of information about an object or scene without physical contact with it. This can be achieved by exploiting the fact that materials comprising the various objects in a scene reflect, absorb, and emit electromagnetic radiation in ways characteristic of their molecular composition and shape. When the radiation captured by sensors is measured at each wavelength over a sufficiently broad spectral band, the resulting spectral signature can be used to uniquely characterize and identify any given materials[1].

However, due to the technical constraints and natural heterogeneity, the spectrum of each pixel is not the pure spectral signature but rather a mixture of several pure spectral signatures, where each represents one of the materials present in that pixel. This fact calls for a method to quantitatively decompose, or unmix, these mixtures. The spectral unmixing is a procedure which decompose a mixed pixel into a set of

constituent spectra, also known as "endmembers", and a set of corresponding fractions, called "abundances", that indicate the proportion of each endmembers in the mixed pixel. In the application of remote sensing, endmembers are usually known as water, soil, metal, plants, etc.[2].

In general, HSI unmixing analysis consists of three steps[3]: Dimension reduction; Endmember extraction; and Abundance estimation. People mainly focus on the second and third steps, as dimensionality reduction is a common data pre-processing step in all signal processing problems. Endmembers generally can be identified by their unique spectral reflectance once detected in high spectral resolution. Extracting such endmember signature from the HSI data, however, is very difficult. In general, the extraction algorithms in literature are based on two criteria: geometry and statistics. Geometry based extraction algorithms follow the insight that the HSI data is embed in a simplex whose vertex are those endmembers we want to extract. Thus endmember extraction problem becomes searching such a simplex. Representative algorithms are Vertex Component Analysis (VCA)[4] which is based on projection, simplex growing algorithm (SGA)[5], sequential maximum angle convex cone (SMACC)[6] based on Maximum-volume, and the minimum volume transform-nonnegative matrix factorization (MVC-NMF)[7]. The key to the application of statistics-based algorithms is that the statistics inferred from the HSI data can provide information about endmembers. Another comprehensible algorithm is dependent component analysis method (DECA)[8], which assumes the abundance vectors are drawn from Dirichlet distribution. DECA then performs a generalized expectation maximization (GEM) algorithm to infer the model parameters.

After extraction of endmember signatures, the last step is spectral unmixing problem, which aim at estimating the abundance  $\mathbf{x}$ . The estimation problem can cast into inverse or regression problem. If there is no constraint on the abundance, the problem can be formulated as a standard Least Square (LS) problem, which has a closed-form solution. However, there are two constraints on abundance in HSI literature, which are abundance nonnegative constraint (ANC) and abundance sum-to-one constraint (ASC), respectively. When both ANC and ASC are activated, the LS becomes fully constrained LS (FCLS). Despite there are no explicit sparse constraints in FCLS, it has been shown [9] that the solutions are indeed sparse under certain conditions. Sparse regression has shown its success in lots of applications, including HSI unmixing in remote sensing domain. Unlike the previous unmixing algorithms, sparse based methods rely on a large spectral library where all possible pure endmember signatures are collected in advance. And the HSI data measured by sensors

is a linear combination of a small set of pure endmembers in that library. The objective then becomes finding the optimal subset of endmembers in that spectral library that can fit the observed HSI reflectance in a linear manner. In literature, greedy algorithms, for example Orthogonal matching pursuit (OMP)[10], and convex relaxations, such as substituting  $\ell_0$ -norm with  $\ell_1$ -norm are common methods to solve the sparsity problems. [11], however, points out that the sparse abundance can be exactly reconstructed by the convex relaxations, if the columns of  $\mathbf{A}$  are incoherent, which violates the fact that spectral signatures are usually highly correlated. The current sparsity research direction, which is called structured sparsity, leverages the prior knowledge about the sparsity patterns in real applications. Successful algorithms based on this direction include SunSAL[12], CLSunSAL[13]. However, the performance of these algorithms can be affected dramatically by noise. Another problem is that the optimization model based unmixing algorithms are usually computational demanding, making them unsuitable for real-time unmixing scenarios.

Recent development of machine learning, especially deep neural network (DNN), has drawn the attention of HSI image processing society, and lots of algorithms have been inspired to achieve quite impressing results. There are, in general, two types of neural networks that can achieve HSI unmixing. The first one is so-called supervised learning networks. In this network, a set of training samples are provided to the network. The networks take as input the HSI reflectance, then through the computation defined in the network, it outputs an estimate of corresponding abundance vector. By minimizing the difference between estimated abundance and ground truth abundance, the parameters in the network are updated. After the training of network converges, a mapping function then is learned, which can map each HSI reflectance into corresponding abundance vector[14]. The drawbacks of this type of method is that it requires a large set of HSI reflectance with corresponding abundance vector as ground truth, which is typically hard to obtain in HSI problem by measurements. One common compromise is to use some existing unmixing algorithms to generate such ground truth. The performance of this type of networks depends heavily on the quality of the training dataset. Another type of neural network is so-called unsupervised learning networks. A typical network of this kind is autoencoder, which composes of two sub-networks, where the first one usually takes as input the HSI reflectance, then outputs a low-dimensional representation known as bottleneck, while the second sub-network maps back to the HSI reflectance. This is also known as self-supervised learning or representation learning. Lots of algorithms based on autoencoder have been proposed [15],[16],[17],[18]. Autoencoder does not acquire the ground truth abundance vector, thus it is very popular in HSI blind unmixing problems. Another useful assumption is that the bottleneck of autoencoder has a natural interpretation of abundance, as it resembles the idea in learning theory, which is a high-dimensional data (HSI data) can be represented as a low-dimensional representations (abundance) given the basis (endmembers). In particular, when the decoder is constructed as a single matrix multiplication, the weights in decoder then can be interpreted as endmember signatures.

One of the most significant problems with these learning based algorithms is that they are known as black box, which makes neural network lack of interpretability. let alone there is no guidance for the construction of network. The design of a network structure therefore requires significant many times of trials. Another disadvantages is that it is usually difficult to make use of prior knowledge about the specific problem at hand to the network construction.

In recent years, [19] and [20] proposes to use the idea of unfolding to unfold an iterative shrinkage thresholding algorithms (ISTA) to a learnable network for the compressive sensing problem. The network is derived from a sparse coding model, thus the final network has good interpretability. A similar idea is exploited in [21] for HSI unmixing problem.

In this paper, we propose two novel network structures for abundance estimation and blind unmixing respectively. For each structure, we propose two different versions for a different preference of model interpretability and model flexibility. Specifically, we start by formulating the HSI unmixing problem as a linear constraint sparse coding model, which is commonly used in sparse unmixing literature. Then we analyze the iterative updating schemes of the famous ADMM algorithm, which has shown of great power in optimization literature, as it requires little assumptions to guarantee the convergence, and it shows fast convergence in practice. Inspired by unfolding network, we propose novel network structures for HSI unmixing that can leverage the benefits of interpretability of model based algorithms and the flexibility of learning based algorithms. The novelty of our works are following.

- 1) We propose two novel neural networks, for abundance estimation and blind unmixing respectively, motivated by ADMM algorithm and Linear mixture model. Each network has two different versions, one of them is built for the preference of model interpretability, while another network is preferred to model flexibility. Nevertheless, all networks have the advantages of model based and learning based algorithms, showing a good network interpretability, fast computation and strong network capacity. Compared to networks unfolded from ISTA, our network structures have much more residual connections, which has been shown in deep learning literature a very powerful structure for image processing. Thus, the proposed networks can achieve faster convergence and improve the performance quite a lot when the size of training dataset is small, both of which are very important in real-time HSI applications.
- 2) We discuss in details the construction of proposed model, as well as the initialization strategies with different level of accessibility to the prior knowledge about endmember signatures and the optimization parameters. We have also shown that every layer of proposed unfolding structures can find corresponding interpretations in machine learning literature. Different from commonly used MSE training objective, we propose to add another two loss terms, abundance angle distance (AAD) and abundance information divergence (AID), which can boost the networks to achieve faster convergence.
- 3) Extensive experiments demonstrate the competitive per-

formance of proposed methods when compared to state-of-art unmixing methods.

The rest of this paper is organized as follows. Section II reviews some related works. In Section III, we show the construction of proposed unmixing networks inspired from unfolding ADMM. The initialization and training strategies are also discussed. In Section IV, extensive experiments are presented to demonstrate the performance of proposed methods. Finally, in Section V, conclusions of our work and future directions are drawn.

## II. RELATED WORK

In this section, we introduce some basic notions and techniques that are related to our work.

### A. Linear Mixture Model

One of the most popular model for hyperspectral unmixing is Linear Mixture Model (LMM)[22]. It Assumes that there is a linear relationship between the fractional abundance of endmembers present in pixel and the spectra in the reflected radiation[2], i.e., the spectrum of a mixed pixel is a linear combination of the endmembers spectra weighted by their corresponding fractional abundance in that pixel. It can be described as following:

$$\mathbf{y} = \mathbf{A}\mathbf{x} + \mathbf{n} \quad (1)$$

where  $\mathbf{y} \in R^{N_B \times 1}$  is the reflectance vector for a specific pixel, therefore  $N_B$  is the total number of bands. Denote  $\mathbf{A} = [\mathbf{a}_1, \dots, \mathbf{a}_{N_E}]$  the mixing matrix, which contains the signatures of the endmembers present in the HSI data, where  $\mathbf{a}_m \in R^{N_B \times 1}$  is the signature vector of the  $m^{th}$  endmember,  $m = 1, \dots, N_E$ , thus totally  $N_E$  endmembers. Let  $\mathbf{x} = [x_1, \dots, x_{N_E}]^T$  be the fractional abundance vector, and  $\mathbf{n} = [n_1, \dots, n_{N_B}]^T$  models additive noise in each band. Given the observed reflectance vector  $\mathbf{y}$ , the objective here is to estimate the appropriate endmember signature matrix  $\mathbf{A}$  and fractional abundance vector  $\mathbf{x}$ . Sometimes, the mixing matrix  $\mathbf{A}$  is known as a priori in the form of spectral library, thus abundance  $\mathbf{x}$  is the only estimation objective. Along with the estimation problem come two physically reasonable constraints: (1) all abundances must be nonnegative,  $x_m \geq 0$ , for  $m = 1, \dots, N_E$ ; and (2) the sum of abundance for every pixel equals to one,  $\sum_{m=1}^{N_E} x_m = 1$ . These two constraints are usually called abundance nonnegative constraint (ANC) and abundance sum-to-one constraint (ASC), respectively.

### B. Linear Unmixing Algorithms

Linear unmixing algorithms usually try to estimate the abundance  $\mathbf{x}$  in the linear model (1), given observation  $\mathbf{y}$  and endmember signature matrix  $\mathbf{A}$  as a priori. There are some algorithms solve the estimation of  $\mathbf{A}$  and  $\mathbf{x}$  simultaneously. For now, let's assume  $\mathbf{A}$  is known. Then the estimation problem becomes a fully constraint least square (FCLS) problem:

$$\min_{\mathbf{x}} \frac{1}{2} \|\mathbf{y} - \mathbf{A}\mathbf{x}\|_2, \text{ s.t., } \mathbf{x} \geq \mathbf{0}, \text{ and } \mathbf{1}^T \mathbf{x} = 1 \quad (2)$$

where  $\|\cdot\|_2$  denote the  $\ell_2$ -norm, and  $\mathbf{1}$  denote the all-one vector. Although there is no explicit sparse constraint in FCLS problem, it has been shown that the solutions are indeed sparse under certain constraints[9].

A sparse generalization of FCLS problem is introduced by adding a sparse constraint explicitly to the objective, giving rise to constraint sparse regression (CSR) problem:

$$\min_{\mathbf{x}} \frac{1}{2} \|\mathbf{y} - \mathbf{A}\mathbf{x}\|_2 + \lambda \|\mathbf{x}\|_1, \text{ s.t., } \mathbf{x} \geq \mathbf{0} \quad (3)$$

where  $\|\cdot\|_1$  denote the  $\ell_1$ -norm,  $\lambda \geq 0$  is a penalty parameter that controls the sparsity of solutions. Note that if the ASC constraint was enforced in (3),  $\ell_1$ -norm  $\|\mathbf{x}\|_1$  would become constant in the feasible set, and FCLS problem would be equivalent to CSR problem. There are some efficient algorithms[23],[24],[25],[13] can solve this type of problems. Among them, SunSAL is one of the most popular sparse unmixing algorithms, which is derived from a famous optimization method, ADMM[26]. In ADMM, problem (3) is solved by introducing an auxiliary variable  $\mathbf{z}$ , which is constrained by  $\mathbf{x} = \mathbf{z}$  and a dual variable  $\mathbf{d}$ , then performing an iterative updating scheme:

$$\mathbf{x}_{k+1} = (\mathbf{A}^T \mathbf{A} + \mu \mathbf{I})^{-1} (\mathbf{A}^T \mathbf{y} + \mu(\mathbf{z}_k + \mathbf{d}_k)) \quad (4)$$

$$\mathbf{z}_{k+1} = \max \left( \text{soft} \left( \mathbf{x}_{k+1} - \mathbf{d}_k, \frac{\lambda}{\mu} \right), 0 \right) \quad (5)$$

$$\mathbf{d}_{k+1} = \mathbf{d}_k - (\mathbf{x}_{k+1} - \mathbf{z}_{k+1}) \quad (6)$$

where,  $\mu \geq 0$  is a free parameter introduced by ADMM. Usually, it is chosen as an upper bound on the largest eigenvalue of  $\mathbf{A}^T \mathbf{A}$ . It is clear that the update expression of  $\mathbf{x}_{k+1}$  performs a weighted least square solution. The update expression of  $\mathbf{z}_{k+1}$  consists of a maximal operation and a soft thresholding operation[27], where the former operator comes from the ANC constraint and the latter is derived from the  $\ell_1$ -norm.  $\mathbf{d}_{k+1}$  is an accumulator for the difference  $(\mathbf{x}_{k+1} - \mathbf{z}_{k+1})$ .

### C. Blind unmixing Algorithms

Blind unmixing algorithms try to estimate the abundance  $\mathbf{x}$  and endmember signature matrix  $\mathbf{A}$  in the linear model (1) at the same time, given the observation  $\mathbf{y}$  only. It is a typical nonnegative matrix factorization (NMF) problem,

$$\min_{\mathbf{X}, \mathbf{A}} \frac{1}{2} \|\mathbf{Y} - \mathbf{A}\mathbf{X}\|_2 + \lambda \|\mathbf{X}\|_1, \text{ s.t., } \mathbf{X} \geq \mathbf{0}, \mathbf{A} \geq \mathbf{0}, \quad (7)$$

where,  $\mathbf{Y}, \mathbf{X}$  are the HSI data and abundance in matrix notation. There are several solutions that can find the  $\mathbf{A}, \mathbf{X}$ , among which the multiplicative update rule[28] is one of the popular way because of its simplicity of implementation. Again, it is an iterative updating scheme, which performs following update,

$$\mathbf{X}_{k+1} = \mathbf{X}_k \odot (\mathbf{A}_k^T \mathbf{Y}) \oslash (\mathbf{A}_k^T \mathbf{A}_k \mathbf{X}_k + \lambda) \quad (8)$$

$$\mathbf{A}_{k+1} = \mathbf{A}_k \odot (\mathbf{Y} \mathbf{X}_{k+1}^T) \oslash (\mathbf{A}_k \mathbf{X}_{k+1} \mathbf{X}_{k+1}^T) \quad (9)$$

where  $\odot$  and  $\oslash$  denote the element-wise multiplication and element-wise division, respectively. Like most iterative algorithms, this is usually computational demanding, making it very slow to achieve convergence.

#### D. Learning based unmixing algorithms

There are, in general, two types of network framework for HSI unmixing problem. The first type of network is known as supervised learning, of which the structure is depicted in Fig. 1. It works as following: Given input  $y$ , it learns a network  $f$  parameterized by  $\theta$  that generates the desired output  $x = f_\theta(y)$ .

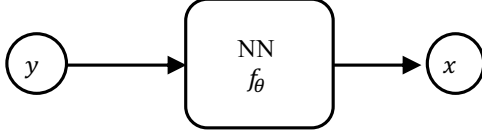


Fig. 1. Framework I. Supervised learning network, which takes input  $y$ , learns a network parameterized by  $\theta$  that generates desired output  $x$ .

For example, [14] is a very early paper introducing neural network into HSI unmixing. [14] firstly trains a traditional autoencoder, from which, after training, the encoder is extracted out and concatenated by a random-initialized classifier. Then this new concatenated network is trained to classify pure endmember data from USGS library while the encoder is fixed as an low-dimensional representation generator for the input HSI spectral vector. [14] argues that although the output of this network is the probability of belonging to each pure endmember from the USGS library, the normalized output vector can be then interpreted as abundance vector for corresponding input spectral vector. However, there are several drawbacks about this algorithm. first of all, it needs the USGS spectral library to provide the pure training data for classifier. Secondly, if the training examples per endmember class is not sufficient, then this classifier could be overfitting very easily. [29] uses the modern convolutional neural network (CNN) to train the classifier given the great success of CNN exploring contextual features of HSI.

The second type of network is so-called autoencoder, which composes of two networks, encoder  $f_\theta$  and decoder  $g_\phi$ . Encoder  $f_\theta$  generates some latent variables  $x = f_\theta(y)$ , which is usually in a lower-dimensional latent space than input  $y$ , while decoder  $g_\phi$  reconstructs input  $y = g_\phi(x)$ , given the latent variables  $x$ . This type of network is illustrated in Fig. 2. Nowadays, more and more algorithms based on the autoencoder framework are proposed as a solver to the HSI unmixing problem due to its unsupervised learning capability.

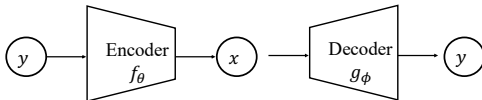


Fig. 2. Framework II. Unsupervised learning networks, which learns a low-dimensional latent space by lossy reconstructions.

Surprisingly, the math expression of neural network and the math for linear unmixing model have a similar structure, which leads to an assumption that if the decoder is constructed as a single-layer linear decoder, then it serves as linear mixing function given the latent variable interpreted as abundance. Then the endmember signature is exactly the weights of

decoder. Another assumption is made based on the fact that since the encoder is trying to unmix the HSI data while the decoder is trying to mix back the HSI data, then the weights of encoder and decoder should be tied since they behave opposite to each other. Endmember extraction algorithms based on these assumptions include [15], [16]. DSCN++[17] utilizes the same idea as Inception Network[30] to obtain a more stable results and proposes a NN-based multinomial mixture model to obtain the corresponding abundance in an unsupervised manner. DAEN[18] proposes to firstly use traditional VCA algorithm to generate a set of pure endmember candidates which is then trained with a stack of autoencoder to generate a good initialization for the parameters in variational autoencoder. By truncating the bottleneck that does not meet the abundance nonnegative constraints and imposing abundance sum to one constraint hardly, VAE is trained to estimate abundance with the minimum simplex volume regularizer.

Recently, uDAS[31] proves that the tied weight assumption and non-negative weight assumption on encoder are not appropriate. Instead, [31] imposes a sparsity constraint on the encoder and a marginalized denoising constraint on the neural network to achieve better unmixing results. [32] use VAE to learn firstly a low-dimension representation of HSI input, then solve an alternating nonlinear least-squares problem by iteratively updating the abundance and endmember in low-dimension representations generated by VAE. EndNet[33] introduces an additional layer using a projection operation instead of inner product, and the loss function in [33] is composed of KL divergence and sparsity penalty on the estimates. These type of methods, however, are known as black box, which means it lacks of interpretability for the architecture and parameters. Another issue is that there is no guideline for the construction of the network.

To tackle the above problem, some model driven neural networks have been proposed. Among them the idea of unfolding has recently drawn the attentions. It is firstly proposed in [19], which proposes to unfold ISTA to a learnable network that can approximate the sparse code. Following this clue, [20] and [34] further unfold ISTA to solve compressive sensing problems. Recently, [21] and [35] also proposes to unfold ISTA to perform HSI unmixing. It replaces the fixed parameters in ISTA with learnable parameters, resulting in an unfolded network, which is learned by minimizing the difference between the estimate abundance by the network and the ground truth. Note that our work is different from them. First of all, in this paper, we propose to unfold ADMM, which is a more stable and faster algorithm than ISTA. It can also be shown in the resulting architectures, where our proposed network has more residual connections than unfolding ISTA. Secondly, based on the interpretation of the network structure, we discuss in details about the initialization strategies which incorporate the prior information of the problem at hand. Another difference is that in [21] and [35], the network is trained using mean squared error (MSE) loss, whereas, in this paper, we propose to add another two loss terms, as MSE is known as not a proper dissimilarity measurement.

### III. UNMIXING NETWORK FROM UNFOLDING ADMM

The idea of unfolding starts from a conventional optimization problem, which is usually solved by iterative updating methods. This kind of iterative method naturally provides a neural network structure which is composed of several layers performing the operation defined by the iterative methods. The network then can be trained via deep learning techniques to estimate the outcomes of the original iterative updating methods. Unlike computational demanding iterative methods, a well trained network is very fast in prediction phase. Following the clue, in this section, we start from the CSR problem and ADMM methods, which inspires to build a new type of neural network architectures for hyperspectral unmixing. The unfolded network structure has a very clear interpretability, which enables to incorporate the prior information about the problem at hand.

#### A. Unfolding Each Step of ADMM as a Network Layer

By inspecting the ADMM solution in (4-6), it consists of 3 updating equations, each of which can be unfolded to a neural network layer that performs the operation defined by the equation. The basic idea is to design, based on these 3 type of layers, a nonlinear feed-forward architecture with a fixed depth and learnable parameters that can be learned to perform hyperspectral unmixing. We now introduce these 3 different type of layers respectively.

1) *X-update Layer*: Let's first unfold the formula (4) at  $(k+1) - th$  iteration. For the purpose of simplifying the formula, Let's first define some notations:  $\mathbf{W}^T = (\mathbf{A}^T \mathbf{A} + \mu \mathbf{I})^{-1} \mathbf{A}^T$  and  $\mathbf{B}^T = (\mathbf{A}^T \mathbf{A} + \mu \mathbf{I})^{-1} \mu$ . Then, (4) can be written as following:

$$\mathbf{x}_{k+1} = \mathbf{W}^T \mathbf{y} + \mathbf{B}^T (\mathbf{z}_k + \mathbf{d}_k) \quad (10)$$

It is clear that this updating expression should accept the up-to-date  $\mathbf{z}_k$  and  $\mathbf{d}_k$  from  $(k) - th$  iteration, as well as the original HSI observation  $\mathbf{y}$ . Then the new estimate  $\mathbf{x}_{k+1}$  is calculated by (10) given  $\mathbf{W}$  and  $\mathbf{B}$ . The idea of unfolding is that, instead of hand-coding  $\mathbf{W}$  and  $\mathbf{B}$ , we use learnable parameters  $\mathbf{W}_{k+1}$  and  $\mathbf{B}_{k+1}$  to play the role of  $\mathbf{W}$  and  $\mathbf{B}$  at  $(k+1) - th$  iteration. Then a computation layer, the structure of which is depicted in Fig. 3, is defined. We name it, *X-update Layer*, as it acts as the role of updating  $\mathbf{x}$  in original ADMM. It takes as input  $\mathbf{z}_k$  and  $\mathbf{d}_k$  as well as  $\mathbf{y}$ . By performing the following computation  $f_X$ :

$$\begin{aligned} \mathbf{x}_{k+1} &= f_X(\mathbf{z}_k, \mathbf{d}_k, \mathbf{y}; \mathbf{W}_{k+1}, \mathbf{B}_{k+1}) \\ &= \mathbf{W}_{k+1}^T \mathbf{y} + \mathbf{B}_{k+1}^T (\mathbf{z}_k + \mathbf{d}_k) \end{aligned} \quad (11)$$

this layer outputs the new estimate  $\mathbf{x}_{k+1}$  given the learnable parameters  $\mathbf{W}_{k+1}$  and  $\mathbf{B}_{k+1}$ . Note that in original unmixing problem, the endmember signature matrix should satisfy  $\mathbf{A} \geq 0$  for physical meanings. In original ADMM context, there is one constraint  $\mu \geq 0$  too. But we do not impose corresponding constraints on  $\mathbf{W}_{k+1}$  and  $\mathbf{B}_{k+1}$  for the purpose of increasing the network's flexibility. Another reason is that the goal of this network is to estimate the abundance vector, not the endmember signature matrix, so there is no need to impose such constraint.

Interestingly, the operation defined in this layer is similar to the well-known *Dense Layer* in deep learning literature, which performs the operation:  $\mathbf{x} = f(\mathbf{y}; \tilde{\mathbf{W}}, \mathbf{b}) = \tilde{\mathbf{W}}^T \mathbf{y} + \mathbf{b}$ , where  $\mathbf{x}$  and  $\mathbf{y}$  are the output and input of dense layer, respectively,  $\{\tilde{\mathbf{W}}, \mathbf{b}\}$  are the learnable parameters. This can be easily verified if we define  $\tilde{\mathbf{W}}^T = [\mathbf{W}_{k+1}^T \quad \mathbf{B}_{k+1}^T]$ ,  $\mathbf{b} = \mathbf{0}$  and  $\tilde{\mathbf{y}} = [\mathbf{y}^T \quad (\mathbf{z}_k + \mathbf{d}_k)^T]^T$ , then the equation (11) can be written in the form:

$$\mathbf{x}_{k+1} = \tilde{\mathbf{W}}^T \tilde{\mathbf{y}} + \mathbf{b} \quad (12)$$

Despite of the operation similarities, the layer defined here is different from dense layer in several perspectives. First of all, the layer operation defined in X-update layer is derived from unfolding an iterative updating algorithms, totally different from the context of dense layer. Secondly, the learnable parameters in X-update layer is interpretable through the definition of  $\mathbf{W}$  and  $\mathbf{B}$ , while the parameters in dense layer are usually lack of interpretability. Another difference is that, it is usually difficult to incorporate the prior information in dense layer, which however is not the case in X-update layer. For example, one can leverage the prior information about endmembers through  $\mathbf{W}$  and  $\mathbf{B}$ .

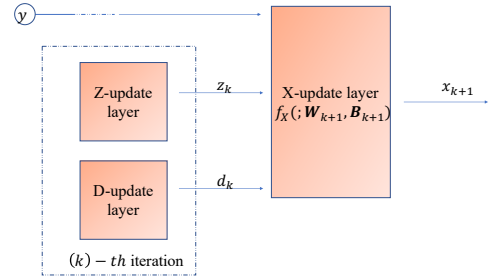


Fig. 3. X-update Layer at  $(k+1) - th$  iteration, which performs operation defined by (11).

2) *Z-update Layer*: Similarly, we check the expression (5) at  $(k+1) - th$  iteration. It is obvious that this formula estimate  $\mathbf{z}_{k+1}$  by performing some sort of nonlinear operations to the up-to-date  $\mathbf{x}_{k+1}$  and  $\mathbf{d}_k$ , given the parameter  $\frac{\lambda}{\mu}$ . Following the idea of unfolding in X-update Layer, we use instead, a learnable parameter  $\theta_{k+1}$  to substitute for  $\frac{\lambda}{\mu}$  at  $(k+1) - th$  iteration. This inspires the construction of a new type of layer, the structure of which is shown in Fig. 4. We name it, *Z-update Layer*, because it resembles the role of updating  $\mathbf{z}$  in original ADMM. It takes as input  $\mathbf{d}_k$  and  $\mathbf{x}_{k+1}$ , which is the output of X-update layer from  $(k+1) - th$  iteration. By performing the following computation  $f_Z$ :

$$\begin{aligned} \mathbf{z}_{k+1} &= f_Z(\mathbf{x}_{k+1}, \mathbf{d}_k; \theta_{k+1}) \\ &= \max(\text{soft}(\mathbf{x}_{k+1} - \mathbf{d}_k, \theta_{k+1}), 0) \end{aligned} \quad (13)$$

this layer outputs the new estimate  $\mathbf{z}_{k+1}$  given the learnable parameter  $\theta_{k+1}$ . Notice that in the original ADMM updating formula, both  $\lambda$  and  $\mu$  are nonnegative. Here we do not impose such constraints to  $\theta_{k+1}$  as it can be automatically learned from the data.

It worth a special attention to the computation  $f_Z$ . If there was no maximal operation, then it reduces to the famous

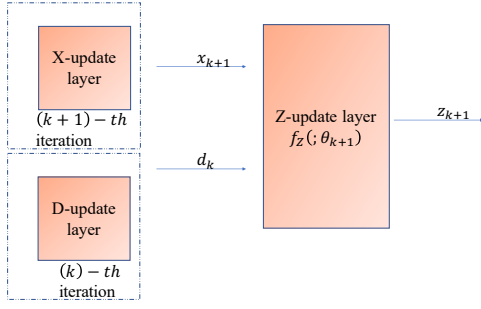


Fig. 4. Z-update Layer at  $(k+1) - th$  iteration, which performs operation defined by (13).

component-wise vector shrinkage function:  $[soft(x, \theta)]_i = sign(x_i) \max(|x_i| - \theta, 0)$ . An illustration of this operation is shown in Fig 5. A straightforward reasoning is that the maximal operation just chunk the negative part of shrinkage function to be 0, satisfying the ANC constraint. This reasoning is also illustrated in Fig 5. A surprising observation is that this chunked shrinkage function is very similar to  $ReLU$ , one of the most commonly used nonlinear activation function in deep learning field:  $ReLU(x) = \max(x, 0)$ . It is not hard to write this nonlinear operation defined by (13) in the form of  $ReLU$ :

$$f_Z(x_{k+1}, d_k; \theta_{k+1}) = ReLU(x_{k+1} - d_k - \theta_{k+1} \mathbf{I}) \quad (14)$$

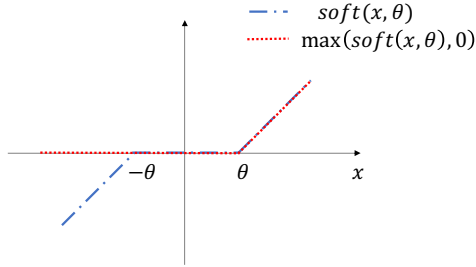


Fig. 5. Soft shrinkage function and Max+Soft shrinkage function.

Note that we start from a conventional optimization problem, arriving at a nonlinear activation function that is similar to the one commonly used in deep learning literature. This further justifies the idea of unfolding an optimization algorithm to a learnable network structure. Here rises another network design choice: whether to use scalar  $\theta_{k+1}$  or vector  $\theta_{k+1}$ . mathematically, this results in whether setting an individual threshold for every component in  $x_{k+1} - d_k$  or setting a common threshold like the ADMM. To be consistent with ADMM, we here use a scalar  $\theta_{k+1}$ .

3) *D-update Layer*: Here left the last updating expression (6). This updating formula, at  $(k+1) - th$  iteration, simply accumulates the difference between up-to-date  $x_{k+1}$  and  $z_{k+1}$ . Inspired by this updating formula, we design a network layer called, *D-update Layer*, as it plays the role of updating  $d$  in original ADMM. The structure of D-update layer is shown in Fig. 6. It takes as input  $x_{k+1}$ ,  $z_{k+1}$ , and  $d_k$ , which are the output of X-update layer at  $(k+1) - th$  iteration, Z-update layer

at  $(k+1) - th$  iteration, D-update layer at  $(k) - th$  iteration, respectively. By performing the following computation  $f_D$ :

$$\begin{aligned} d_{k+1} &= f_D(x_{k+1}, z_{k+1}, d_k; \eta_{k+1}) \\ &= d_k - \eta_{k+1}(x_{k+1} - z_{k+1}) \end{aligned} \quad (15)$$

this layer outputs the new estimate  $d_{k+1}$  given the learnable parameters  $\eta_{k+1}$ . Here we introduce  $\eta_{k+1}$  to increase the network flexibility. It acts like the step-size in iterative updating schemes. Following the clue of X-update layer and Z-update layer, this D-update layer must can find a counterpart in the literature of deep learning. We will discuss this latter when putting together the separate layers as a block.

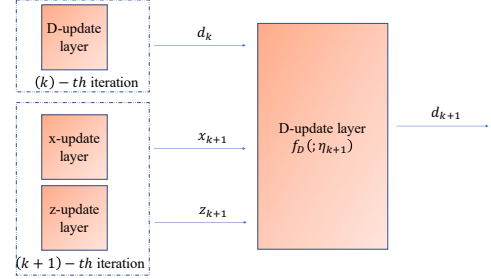


Fig. 6. D-update Layer at  $(k+1) - th$  iteration, which performs operation defined by (15).

### B. Iteration blocks combing all Layers

The 3 different type of layers inspired by ADMM, together form an iteration block, the structure of which is shown in Fig. 7. Each iteration in original ADMM now is unfolded as a block of layers consists of X-update layer, Z-update layer, and D-update layer. Different from ADMM, which use hand-coded parameters  $\{A, \mu, \lambda\}$ , the proposed iteration block, at  $k - th$  iteration block, uses learnable parameters  $\Theta_k = \{W_k, B_k, \theta_k, \eta_k\}$ ,  $k = 1, \dots, I$ , where  $I$  is the total number of iteration blocks. The value of  $\Theta_k$  can be automatically determined from the HSI data. One of the benefits of using learnable parameterization is that it can use less number of iteration blocks than the iterations needed for ADMM.

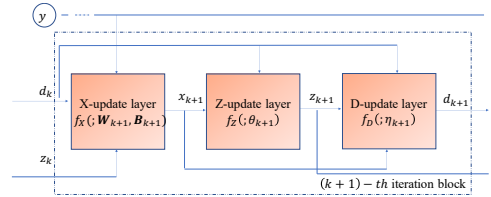


Fig. 7. One iteration block composes of X-update Layer, Z-update Layer and D-update Layer.

Another interesting observation from Fig. 7 is that there are shortcuts and residual blocks in this ADMM inspired block structure. Specifically, at  $(k+1) - th$  block, the input of X-update layer comes from  $z_k$ ,  $d_k$  and  $y$ , which is the output of Z-update layer and D-update layer from  $(k) - th$  block, and the HSI data. In the meantime, the input of Z-update layer comes from  $x_{k+1}$  and  $d_k$ , and the input of D-update layer comes from  $d_k$ ,  $x_{k+1}$  and  $z_{k+1}$ . It can be seen

from Fig. 7 that D-update layer resembles the idea of using shortcut[36], which introduce a skip connection from the input to the output of the block. In addition, the X-update layer and Z-update layer also include skip connections from each other. Together, these 3 layers form a residual block. The idea of using shortcuts and residual block has been shown beneficial to both network training in deep learning literature[37] and image processing for tasks like image denoising[38], image super-resolution[39][40]. It has been shown in [37] that, the residual block can take advantages of hierarchical features and significantly improves the performance for image processing tasks. It is super interesting that we construct a network from unfolding ADMM, which turns out to be a structure contains both skip connections and residual block, which are powerful techniques in deep learning literature.

### C. Unmixing Networks for Abundance Estimation

In this subsection, we discuss in details the network structures for abundance estimation and corresponding initialization and training strategies.

It is worth noting that the parameters  $\{\mathbf{A}, \mu, \lambda\}$  are fixed for all iterations in original ADMM. In consistent with this shared parameterisation characteristic, we introduce our first type of unfolding ADMM based unmixing network for abundance estimation, or *U-ADMM-AENet-I* in short. The overall structure of U-ADMM-AENet-I is shown in Fig. 8a. Here we only show the unfolding for three consecutive iterations. Note that U-ADMM-AENet-I uses the shared layers across iteration blocks. In other words, the learnable parameters are tied across iteration blocks,  $\Theta_k = \Theta' = \{\mathbf{W}', \mathbf{B}', \theta', \eta'\}, \forall k \in [1, I]$ . In this case, there are totally  $(N_E^2 + N_E N_B + 2)$  learnable parameters in U-ADMM-AENet-I, of which  $N_E^2$  parameters are from matrix  $\mathbf{B}'$ ,  $N_E N_B$  parameters are from matrix  $\mathbf{W}'$ , and plus two scalars  $\theta', \eta'$ . It is interesting that this shared parameterization, resembles again, the well-known Recurrent neural network (RNN) in deep learning literature, where the layers are also shared.

To increase the network capacity and flexibility of the structure, we introduce another type of unfolding ADMM based unmixing network for abundance estimation, or *U-ADMM-AENet-II* in short. The main difference from U-ADMM-AENet-I is that this network structure allows the parameters to be untied, i.e., each block  $k$  has individual parameters  $\Theta_k$ . This unshared network structure is illustrated in Fig. 8b. In this case, the network reduces to a feed-forward network. And the number of learnable parameters,  $\Theta = \{\Theta_k\}_{k=1}^I$ , increases to  $(N_E^2 + N_E N_B + 2)I$ , as there are totally  $I$  iteration blocks, for which each has  $(N_E^2 + N_E N_B + 2)$  learnable parameters in  $\Theta_k = \{\mathbf{W}_k, \mathbf{B}_k, \theta_k, \eta_k\}$ . While U-ADMM-AENet-I has the advantages of approaching original ADMM, U-ADMM-AENet-II increases the flexibility and approximation capability of the network.

After constructing the networks, we now discuss in details the initialization strategies. Note that at the beginning of the networks, i.e.,  $(1) - th$  iteration block, we do not have access to  $\mathbf{z}_0$  and  $\mathbf{d}_0$ . Like commonly did in iterative updating schemes, we initialize  $\mathbf{z}_0 = 0$  and  $\mathbf{d}_0 = 0$ . This initialization

is reasonable, because in conventional ADMM, we usually start the algorithm by initializing them to be zero. It is also noticeable that in ADMM, we have introduced an auxiliary variable  $\mathbf{z}$  to take responsibilities for satisfying the  $\ell_1$ -norm and ANC constraint. Thus the output layer of our model must be Z-update layer. In addition, as we do not impose ASC constraint at the very beginning of the unmixing model, we need to normalize the output of our network to satisfy ASC constraint.

In machine learning literature, the parameters in a network are usually randomly initialized, because the parameters do not have any meaningful interpretations to the problem at hand. Although this allows the network to be a general solver for different kinds of problems, it also makes it very hard to incorporate the prior information about specific problem. In this paper, depending on different level of the accessibility to prior information, we propose to use corresponding initialization strategies to give the proposed network a warm start. Note that the strategies introduced below are applicable to all the networks proposed in this paper. First of all, it is noticeable that the initialization of parameters in  $\Theta_k$ , except for  $\eta_k$ , can be achieved through the definition of  $\mathbf{W}_k, \mathbf{B}_k, \theta_k$ , once given  $\{\mathbf{A}, \mu, \lambda\}$ . Thus the key of initialization is to determine the value of these parameters. Notice  $\lambda$  is the sparsity penalty, it is predefined by the model.  $\mu$  is a parameter introduced by ADMM, which usually depends on the largest eigenvalue of  $\mathbf{A}^T \mathbf{A}$ . At this point, the initialization strategy lies on the accessibility of  $\mathbf{A}$ . If we have perfect access to the prior knowledge about endmember signature matrix  $\mathbf{A}$ , we can immediately initialize the parameters using the corresponding definitions. If, however, without  $\mathbf{A}$ , we propose to use existing algorithm to generate an estimate of the endmembers, such as VCA. This strategy can give the network a warm initialization, although  $\mathbf{A}$  is just an estimation of the ground truth value, boosting the convergence of network training. Notice that there is no corresponding parameters in ADMM for  $\eta_k$ , we just initialize it to be equal to 1, as it represents updating step size. It is easy to verify that using the initialization strategies introduced above, an U-ADMM-AENet with  $I$  iteration blocks is just an unfolded version of ADMM algorithm with  $I$  iterations. This is one of reasons that our model can achieve fast convergence and is easy to train. Compared to random initialization strategy which is commonly used in deep learning literature, incorporating the prior knowledge can boost the network training to be easier, thus achieve faster convergence, and reduce the reliance on large training examples.

Now let's discuss about the training strategies. Once we have settled down the network, commonly, in unfolding literature, people choose MSE-type of loss function to train the network in a supervised way. In other words, we need some training dataset  $D = \{\mathbf{y}_i, \mathbf{x}_i\}_{i=1}^N$ . For each pixel  $i$  in  $D$ , we know the HSI spectrum  $\mathbf{y}_i$  and its corresponding abundance vector  $\mathbf{x}_i$ . This assumption is not hard to satisfy as it can be acquired by either measurements or any existing unmixing techniques. For example, we could utilize FCLS solutions as an estimate of  $\mathbf{x}_i$  when its true value is unavailable. One of





Fig. 8. Overall structure of U-ADMM-AENet from unfolding ADMM. (a) is the overall structure of U-ADMM-AENet-I, where the layers are shared across blocks. (b) is the overall structure of U-ADMM-AENet-II, where the layers are untied across blocks.

the commonly used loss is MSE:

$$MSE(\{\mathbf{x}_i, \tilde{\mathbf{x}}_i\}_{i=1}^N) = \frac{1}{N} \sum_{\{\mathbf{y}_i, \mathbf{x}_i\} \in D} \|\mathbf{x}_i - \tilde{\mathbf{x}}_i\|_2^2 \quad (16)$$

where,  $\tilde{\mathbf{x}}_i$  is the estimate abundance vector for pixel  $i$ , which is the output of the network given  $\mathbf{y}_i$ .

However, it is commonly recognised that MSE is not a robust measurements for dissimilarity. Here, in this paper, we propose to add another two dissimilarity measurements: abundance angle distance (AAD) and abundance information divergence (AID). AAD is a high-dimensional extension of the geometric angle in the following form:

$$AAD(\mathbf{x}_i, \tilde{\mathbf{x}}_i) = \cos^{-1} \left( \frac{\mathbf{x}_i^T \tilde{\mathbf{x}}_i}{\|\mathbf{x}_i\|_2 \|\tilde{\mathbf{x}}_i\|_2} \right) \quad (17)$$

AID is a metric inspired by information theoretic measure. The abundance vector itself is a set of proportional number, thus it can be interpreted as a probability distribution. A natural reasoning is that the dissimilarity between two probability distributions can be measured by KL divergence:

$$KL(\mathbf{x}_i | \tilde{\mathbf{x}}_i) = \sum_{m=1}^{N_E} \left( x_{i,m} \log \left( \frac{x_{i,m}}{\tilde{x}_{i,m}} \right) \right) \quad (18)$$

where  $x_{i,m}$  is abundance of  $m^{th}$  endmember at pixel  $i$ . A problem of KL divergence is that it is asymmetric. As a result, people usually use following measure:

$$AID(\mathbf{x}_i, \tilde{\mathbf{x}}_i) = KL(\mathbf{x}_i | \tilde{\mathbf{x}}_i) + KL(\tilde{\mathbf{x}}_i | \mathbf{x}_i) \quad (19)$$

To fit in the loss function which is measured over a set of training examples, AAD and AID is also averaged out over the dataset. The final loss function of our proposed model is:

$$L_{\Theta} = \alpha_1 MSE + \alpha_2 MAAD + \alpha_3 MAID \quad (20)$$

where,  $\Theta$  is the set of all learnable parameters of the network.  $\alpha_1, \alpha_2, \alpha_3$  are the weights of corresponding loss term. In this paper, we set  $\alpha_1 = 1.0, \alpha_2 = 1e-7, \alpha_3 = 1e-5$ . *MAAD* stands for mean AAD which is the AAD averaged out over dataset. *MAID* follows *MAAD*.

#### D. Unmixing Networks for blind unmixing

In this subsection, we introduce the details about the proposed unmixing networks for blind unmixing.

Inspired by the above abundance estimation network, we can add another linear layer at the end of the network, which performs following operation,

$$\tilde{\mathbf{y}} = \tilde{\mathbf{A}} \tilde{\mathbf{x}} \quad (21)$$

where,  $\tilde{\mathbf{A}}$  is the learnable parameters in this layer. By enforcing  $\tilde{\mathbf{y}}$  to reconstruct the original HSI data  $\mathbf{y}$ , the parameter  $\tilde{\mathbf{A}}$  then could be interpreted as the endmember signature matrix  $\mathbf{A}$ . To ensure that  $\tilde{\mathbf{A}}$  is physical feasible, we need to add a nonnegative constraint on  $\tilde{\mathbf{A}}$ . Corresponding to the U-ADMM-AENet-I and U-ADMM-AENet-II, we hereby introduce two blind unmixing networks, U-ADMM-BUNet-I and U-ADMM-BUNet-II, whose structures are shown in Fig. 9.

This type of blind unmixing network resembles the autoencoder structure in machine learning literature, where the encoder projects the input into a latent code, and the decoder projects back the latent code into input. One of the advantages of this autoencoder structure is that it does not rely on any ground truth to train the network, thus it is totally unsupervised. Different from the conventional autoencoder, the proposed encoder in this paper is derived from optimization algorithm ADMM. Therefore, it has much stronger interpretability. Similar to the abundance estimation network, here we could initialize the parameters of the network using the same strategies given different level of prior information. But the training strategy is different from previous one. Here we use only MSE loss term for the reconstruction  $\mathbf{y}$  in this blind unmixing network. There are two reasons for not including the other two loss terms. First of all, the goal of blind unmixing network is to estimate the abundance  $\mathbf{x}$  and endmember  $\mathbf{A}$ , not to reconstruct the HSI data  $\mathbf{y}$ . Secondly, a perfect reconstruction of  $\mathbf{y}$  will usually cause overfitting, as  $\mathbf{y}$  is usually a noisy observation.

## IV. EXPERIMENTS

In this section, extensive experiments on both synthetic data and real hyperspectral data are present to demonstrate the effectiveness of proposed methods. We start this section by first introducing the performance metrics adopted in this paper. Then we compare our proposed methods with competitors qualitatively and quantitatively.

#### A. Performance metrics

In this subsection, we introduce some commonly adopted dissimilarity measurements to evaluate the quality of estimate abundance vectors and estimate endmember spectral signatures. In short, the metrics, root mean square error (RMSE), abundance angle distance (AAD), abundance information divergence (AID), and spectral angle distance (SAD) are adopted.

RMSE is perhaps the most popular dissimilarity measurement. It measures the difference between true abundance





Fig. 9. Overall structure of U-ADMM-BUNet from unfolding ADMM. (a) is the overall structure of U-ADMM-BUNet-I, where the layers are shared across blocks. (b) is the overall structure of U-ADMM-BUNet-II, where the layers are untied across blocks.

vector  $x_i$  of pixel  $i$  and its estimation  $\tilde{x}_i$  using following expression:

$$RMSE_i = \sqrt{\frac{1}{N_E} \sum_{m=1}^{N_E} (x_{i,m} - \tilde{x}_{i,m})^2} \quad (22)$$

Geometric-based measurements, AAD, and information-based measurements, AID, as introduced in the construction of loss function, evaluate the dissimilarity between estimated abundance vector and ground truth using expressions (17) and (19).

SAD measures the dissimilarity between the true endmember spectral signature  $a_m$  and its estimate  $\tilde{a}_m$  using the same expressions as (17). The final metrics that measures the quality of estimate abundance vectors are acquired by taking the mean value over the whole evaluation dataset, while the final metrics about endmember spectral signatures are averaged over all endmembers. The smaller the metrics, the better the performance of unmixing algorithms.

### B. Abundance Estimation Comparison Using Synthetic Data

In this section, We will compare the abundance estimation performance of proposed methods with traditional sparse unmixing algorithms: SunSAL[25], as well as unfolding based learning algorithms: MNN-AE-1 and MNN-AE-2[35], using synthetic dataset. Note that we do not involve traditional learning based algorithms, such as pixel-based CNN[29], because it has been verified in [35] that the performance of MNN-AE is better than pixel-based CNN. In this paper, we follow the synthetic HSI data generation in [41]. This generation composes of two sub-steps: endmember generation and abundance generation.

- 1) Endmember generation. In this experiments, we use the spectral library which is a dictionary of minerals selected from the famous USGS library denoted as splib06[42]. It collects the spectral reflectance values in 224 channels, ranging from 0.4 nm to 2.5 nm. After discarding some bad channels, there are 208 bands left. We randomly select 6 endmembers from this library, thus this endmember generation procedure outputs an endmember matrix consists of 6 endmembers recorded at 208 bands. The signature of these 6 endmembers are shown in Fig. 10.
- 2) Abundance generation. The abundances are generated by first extracting  $a^2$  disjoint patches from a synthetic image of size  $a^2 \times a^2$ . Thus each patch has size  $a \times a$ . For each patch, we randomly choose two endmembers, with which we fill in all the pixels within this patch.

The fractions for these two endmembers are  $\gamma$  and  $1 - \gamma$  respectively. In order to generate a highly mixed synthetic image, the abundance map is convolved with a Gaussian filter of size  $(a+1) \times (a+1)$  whose variance is equal to 2. The ASC constraint is satisfied by re-scaling each pixel. In the following experiments, we set  $a = 10$  and  $\gamma = 0.8$ .

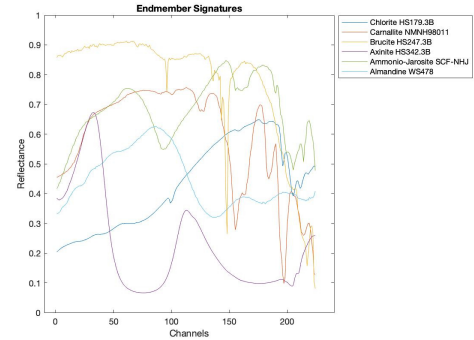


Fig. 10. Endmember signatures for synthetic data.

A subsequent data processing is to contaminate the clean HSI data with additive white Gaussian noise (AWGN). The purpose of this procedure is to verify the robustness of unmixing algorithms to noise. In general, the signal is corrupted with a given signal-to-noise ratio (SNR), which is defined as following:

$$SNR = 10 \log_{10} \frac{E[y^T y]}{E[n^T n]} \quad (23)$$

where, the numerator is known as the power of signal  $y$ , while the denominator is known as the power of noise  $n$ . Then, the training pixels will be randomly picked from the synthetic HSI data, while all synthetic data will be used for evaluation. In this synthetic comparison, we assume the true endmember signatures are available for all algorithms, and the learning based algorithms are trained with ground truth abundance vector. This experiment is to test the performance of various algorithms when perfect prior knowledge is available.

1) *Impact of Training Epochs:* In this experiment, we will evaluate the impact of training epochs on the unmixing performance of unfolding based learning algorithms: the two types of U-ADMM-AENet, and the two types of MNN-AE. In machine learning literature, it can be used as a metric to measure the convergence speed of a learning algorithm. Specifically, the synthetic data are polluted with noise that leads to  $SNR = 15$ . The training dataset of size 1000 are pixels randomly chosen from the synthetic HSI data.

The whole synthetic data are used as evaluation dataset. The number of iteration blocks are set as 2 both for the proposed methods and MNN-AE. In the proposed model, we train the network using Adam optimizer with learning rate set to  $1e-4$ , and batch size set to 64. For MNN-AE, we use the default optimizer settings as introduced in the original papers [35] [21]. All networks are trained with epochs varying from 0 to 500. The results are shown in Fig 11. Note that the AAD is reported in degree, not in radian. It is clearly shown that the proposed methods can achieve convergence with 100 training epochs, while MNN-AE network usually needs 300 epochs to achieve the optimal performance, almost 3 times the epochs need for proposed methods. When the training epochs are large enough, both type of networks achieve a similar performance on abundance estimation. The fast convergence property of proposed methods actually comes from two facts. The first one is that we are unfolding an ADMM optimizer, which is usually very fast in practice. Another reason is that we adopt a weighted loss between RMSE, AAD and AID, each of which is a dissimilarity measurement from different perspectives. The final performances are similar because both networks are unfolded from optimization solvers and there is no clear dominant among them in terms of final performance. In the following experiment, unless specific descriptions, we will set the training epochs as 300 for a fair comparison.

2) *Impact of Number of Iteration Blocks:* In this experiment, we will demonstrate the impact of number of iteration blocks on the unmixing performance of unfolding based learning algorithms. In particular, we use a contaminated synthetic data  $SNR = 15$ , of which 1000 randomly chosen pixels are used as training dataset. All networks are trained with 300 epochs and batch size 64. The remaining training details are the same as the one used in previous experiment. The number of iteration blocks range from 1 to 7. The final results are shown in Fig. 12. It is usually the case that with deeper architectures, the network can achieve better performance due to the increasing network capacity. It can be seen that with deeper architectures, all networks, except for U-ADMM-AENet-I, indeed perform better. This may be due to the fact that the U-ADMM-AENet-I posses both the residual block structure and recurrent network structure, which will make it unstable to train with increasing iteration blocks. But, when the number of iteration blocks are small, all networks can achieve a similar performance. The benefits from constructing a deeper network are very limited. This results further demonstrate that with unfolded structure, the network becomes much more interpretable, thus can achieve a reasonable performance even with shallow structure. As it is well known in machine learning literature, that with deeper structure, the network will become much harder to train, this unfolded type of network can avoid such problem. For the sake of structure simplicity and fair comparison, in the following experiment, all the network are set as 2 iteration blocks. Note that the U-ADMM-AENet-I can achieve better performance with 1 iteration blocks.

3) *Impact of Training Size:* In this experiment, we will evaluate the impact of the size of training dataset on the unmixing performance of unfolding based learning algorithms. As above experiments, we use a noisy synthetic data  $SNR = 15$ .

All networks are composed of 2 iteration blocks and trained with 300 epochs and batch size 64. The remaining training details are the same as above. The size of training dataset changes from 256 to 4096. The final results are shown in Fig. 13. Surprisingly, When the size of training dataset are very small, for example 256, the proposed network can achieve almost 2-3 times better performance than MNN-AE. This may be due to the fact that the network unfolded from ADMM have much residual connections, which have been shown in image processing literature that this will make network more efficient as it forces the network to learn only the difference between the input and the output. It is not hard to see that, all networks benefit from more training data, and eventually achieve a similar performance. This further demonstrates that the proposed network is much more efficient than MNN-AE, as it can achieve quite impressive performance even with very small training dataset. This will make the proposed network much more applicable in real applications as acquiring ground truth is typically not easy.

4) *Impact of Noise:* In this experiment, we illustrate the impact of noise on the unmixing performance of unfolding based learning algorithms and traditional sparse unmixing algorithms, SunSAL. All the synthetic data are used for training and the final metrics are also evaluated on all synthetic pixels. As before, all networks are composed of 2 iteration blocks and trained with 300 epochs and batch size 64. The remaining training details are the same as above. The synthetic dataset are contaminated with different level of AWGN noise, leading to  $SNR = [15, 20, 25, 30, inf]$ . It can be seen from Fig. 14, that, when SNR is low, both proposed network can achieve better performance than MNN-AE. In particular, U-ADMM-AENet-II reduces the error by 25 percent when SNR is 15. Note that U-ADMM-AENet-I can achieve better performance with 1 iteration block. It is obvious that with larger SNR, all networks perform better and eventually achieve a similar performance. As the traditional sparse unmixing algorithm SunSAL is a direct application of ADMM, it acts as a baseline in this comparison. This experiment proves that our proposed network is more robust to noise when compared to state-of-art algorithms.

### C. Abundance Estimation Comparison Using Real Hyperspectral Dataset

In this section, We compare the abundance estimation performance of proposed methods with competitors in real hyperspectral dataset. In short, we adopt the well-known Jasper Ridge [43], and Urban [44],[45], dataset for HSI unmixing. In this experiment, we assume the true endmember signatures are available to all methods. All competitors use the default settings introduced in the original papers. For learning based algorithms, U-ADMM-AENet, and MNN-AE, we train them with ground truth abundances. We do not consider the case of imperfect prior knowledge, where the true endmember signatures and abundances need be estimated via existing unmixing algorithms. One of the reason is that, as this case would be considered in the following blind unmixing experiments, there is no need to take this case into consideration here.

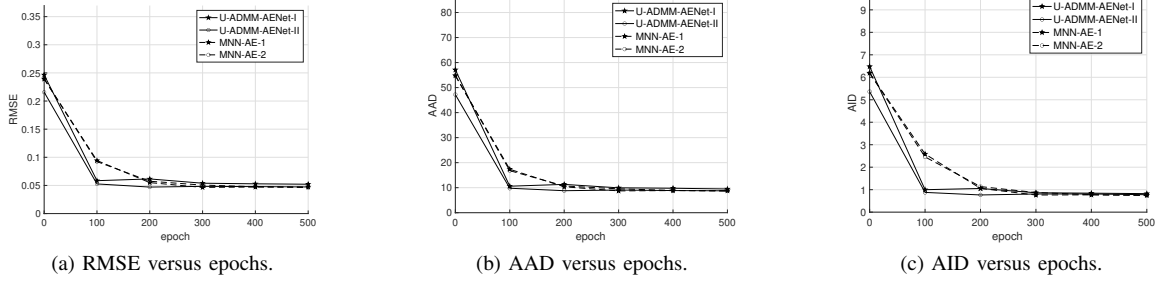


Fig. 11. The impact of training epochs on the performance of abundance estimation. (a) RMSE. (b) AAD in degree. (c) AID.

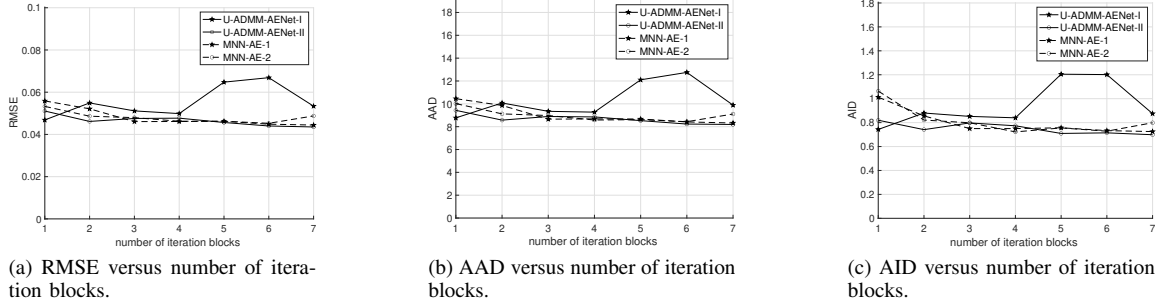


Fig. 12. The impact of number of iteration blocks on the performance of abundance estimation. (a) RMSE. (b) AAD in degree. (c) AID.

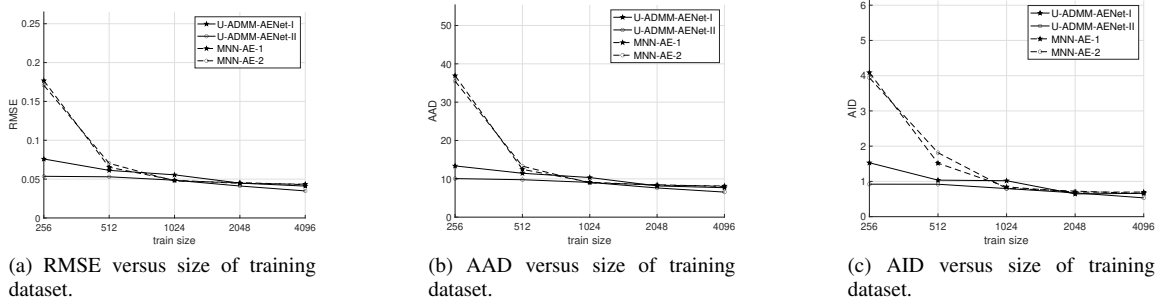


Fig. 13. The impact of size of training dataset on the performance of abundance estimation. (a) RMSE. (b) AAD in degree. (c) AID.

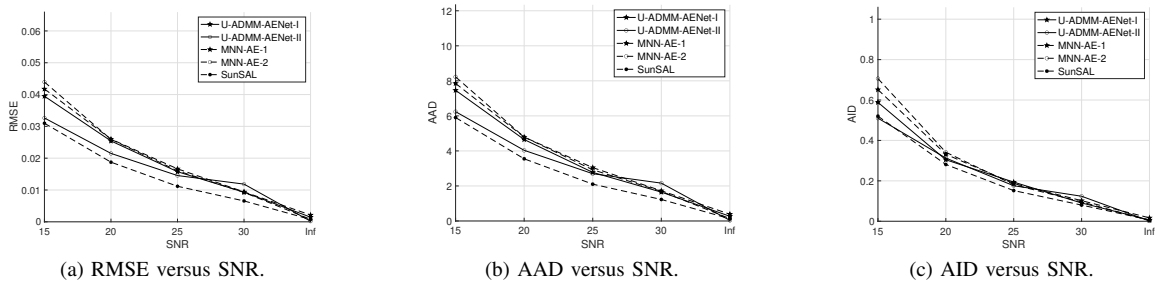


Fig. 14. The impact of SNR on the performance of abundance estimation. (a) RMSE. (b) AAD in degree. (c) AID.

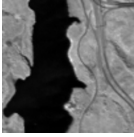
Another reason is that, since the abundance estimation network is supervised, the performance of the network is bounded by the quality of the training dataset. Therefore, comparing the performance of supervised networks trained with imperfect training dataset would be essentially comparing the quality of the training dataset. For each dataset, we randomly choose 256 pixels as training dataset and all networks are trained to achieve convergence. This is to test the performance in the

case where there are very little ground truth available. All algorithms run five times and the average metrics are reported.

1) *Jasper Ridge*: Jasper Ridge is a widely used HSI data in lots of hyperspectral literature. In this, scene, there are totally  $512 \times 614$  pixels, each of which is recorded at 224 channels ranging from 380 nm all the way up to 2500 nm, with a spectral resolution of 9.46 nm. Generally, a sub-image of  $100 \times 100$  pixels, whose 80th channel image is shown in Fig.

TABLE I  
AVERAGED RMSE, AAD (IN DEGREES), AID BY DIFFERENT ALGORITHMS ON JASPER RIDGE AND URBAN. THE BEST RESULTS ARE IN BOLD.

Dataset	Metrics	SunSAL	MNN-AE-1	MNN-AE-2	U-ADMM-AENet-I	U-ADMM-AENet-II
Jasper Ridge	RMSE	0.0612	0.1285	0.1262	0.0545	<b>0.0214</b>
	AAD	7.9068	17.9929	17.4182	7.0709	<b>2.7447</b>
	AID	0.4564	2.1823	2.1215	0.6125	<b>0.1630</b>
Urban	RMSE	0.1679	0.2416	0.2387	0.0886	<b>0.0417</b>
	AAD	25.1087	36.2268	35.6648	12.6038	<b>5.6651</b>
	AID	4.5491	4.7990	4.7601	1.3534	<b>0.3090</b>



(a) Jasper Ridge



(b) Urban

Fig. 15. HSI image at 80th channel. (a) Jasper Ridge. (b) Urban.

15a. are considered due to the complexity of original image, Channels 1-3, 108-112, 154-166 and 220-224 are removed due to dense water vapor and atmospheric effects, leaving 198 channels used for hyperspectral analysis. There are four endmembers reside in this scene: Road, Soil, Water, Tree. The final metrics are reported in table I, where the best performance is in bold. It can be seen that the proposed U-ADMM-AENet achieve the best performance even it is trained with very small dataset. The abundance maps of various algorithms on Jasper Ridge are illustrated in Fig. 16. The same as the performance metrics, the proposed U-ADMM-AENet show better estimation than other algorithms.

2) *Urban*: Urban is one of the most adopted dataset in HSI unmixing field. It consists of  $(307 \times 307)$  pixels, with a spatial resolution of  $2 \times 2 m^2$ . The image of Urban at 80th channel is shown in Fig. 15b. The spectral reflectance is sensed at 210 wavelengths covering from 400 nm to 2500 nm, with a spectral resolution of 10 nm. As a common preprocessing for HSI unmixing analysis, the channels 1-4, 76, 87, 101-111, 136-153 and 198-210 are discarded, due to the dense water vapor and atmospheric effects. As a result, there are 162 channels remaining for subsequent analysis. There are three versions of ground truth coupled with the dataset. In this paper, we use the one contains four endmembers: Asphalt, Grass, Tree and Roof. The final performance metrics are reported in Table I, where the best one is in bold. Again, the proposed network have the best estimation among the competitors. The qualitative comparison of abundance maps are shown in Fig. 17. It can be seen that the proposed networks show an quite impressive estimation even it is trained with a very small dataset.

#### D. Blind Unmixing Comparison Using Synthetic Data

Now we evaluate the performance of proposed blind unmixing networks, U-ADMM-BUNet, on synthetic data, which are generated using the same procedure introduced in abundance estimation comparison. In particular, we compare with learning based blind unmixing algorithms, uDAS[31], MNN-BU[35], and traditional nonnegative matrix factorization (NMF)-based algorithms, matrix-vector nonnegative tensor factorization (MV-NTF)[46]. All models use the default hyperparameter settings proposed in their original papers. In this blind unmixing comparison, we assume not perfect prior knowledge is available, and the parameters of U-ADMM-BUNet are initialized using the proposed strategies. Note that MNN-BU is proposed to be initialized with the result of  $L_{1/2}$  unmixing method, which we cannot find corresponding code. Thus we initialize MNN-BU with the same strategies in this paper, which is also more fair for comparison. Developed from NMF-based methods, MV-NTF decomposes a third-order tensor into the sum of several component tensors, with each component tensor being the outer product of a vector (endmember) and a matrix (corresponding abundances). All the learning based unmixing algorithms, uDAS, MNN-BU, including the proposed network U-ADMM-BUNet, are developed from the famous autoencoder structure, in which encoder projects the spectral reflectance of a pixel onto a latent code, which is interpreted as corresponding abundance, then decoder projects the abundance back onto the spectral reflectance. By enforcing one layer of linear operation in the decoder, the weight of decoder then is interpreted as the endmember signature. The different structures of autoencoder and training strategies promote different algorithms. While uDAS is derived from traditional autoencoder perspectives, MNN-BU and proposed U-ADMM-BUNet are both derived from unfolding an LMM and optimization solvers. As the proposed methods are derived from ADMM, which is a fast algorithm with guarantee of convergence, it enjoys the benefits from ADMM and shows totally different structure from MNN-BU.

1) *Impact of Training Epochs*: In this experiment, we will evaluate the impact of training epochs on the unmixing performance of proposed U-ADMM-BUNet and the two types of MNN-BU. The less epochs it takes, the faster the learning algorithm converges. Specifically, the synthetic noisy HSI data

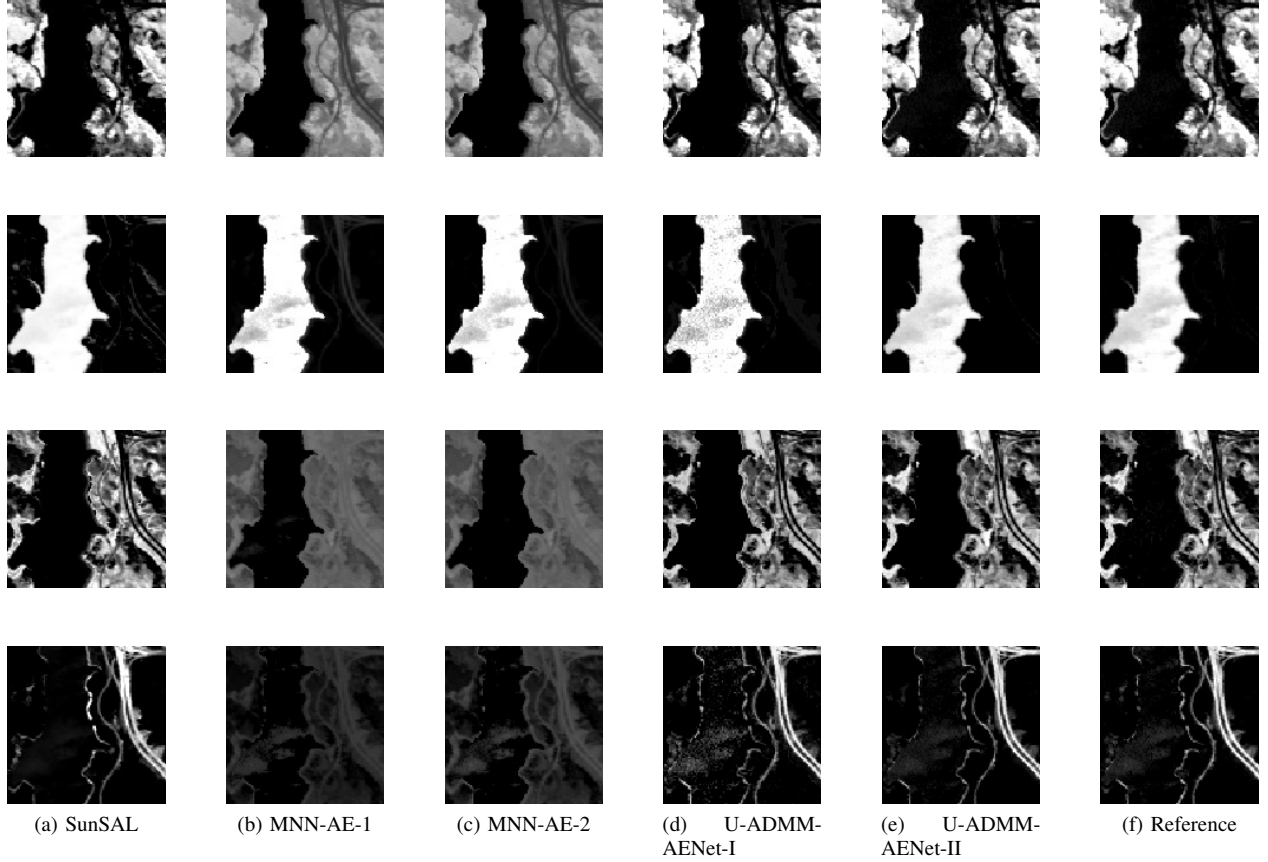


Fig. 16. Results of abundance estimation by different methods on Jasper Ridge dataset. From top to bottom: Tree, Water, Soil and Road. (a) SunSAL. (b) MNN-AE-1. (c) MNN-AE-2. (d) U-ADMM-AENet-I. (e) U-ADMM-AENet-II. (f) Reference.

have  $SNR = 25$ , from which 1000 randomly picked pixels compose the training dataset. The whole synthetic data will be used as evaluation dataset. The number of iteration blocks for all methods are set as 1. All networks are trained with epochs varying from 0 to 1000. The results are shown in Fig 18. Note that the SAD is reported in degrees, not in radians. Again, the proposed methods can achieve a quite good performance with 100 epochs, while MNN-BU need much longer epochs to achieve convergence. The fast convergence property again benefits from the structure of unfolding ADMM. With large enough epochs, all networks show a similar performance, which is reasonable as all networks are unfolded from optimization solvers. It is noticeable that, U-ADMM-BUNet-II and MNN-BU-2, both of which have a shared layer structure, are unstable when the training epochs increase, this may be due to the same reason which cause the unstable performance of U-ADMM-AENet-I. For this reason, in following experiments, we only show comparison results for those with unshared layer structures.

2) *Impact of Number of Iteration Blocks:* In this experiment, we will evaluate the impact of number of iteration blocks on the unmixing performance of unfolding based learning algorithms. As before, we use a contaminated synthetic HSI data with  $SNR = 25$ , of which 1000 randomly chosen pixels are used as training dataset. All networks are trained to achieve convergence. The number of iteration blocks range from 1 to

7. The final results of SAD and RMSE are shown in Fig. 19. It is clear that in most case, the proposed U-ADMM-BUNet-II achieves better SAD and RMSE than MNN-BU-2, given same number of iteration blocks. This benefits from the fact that the network unfolded from ADMM has stronger capacity than network unfolded from ISTA. Moreover, compared with MNN-BU-2, the proposed method are relatively more stable with varying depth. Nevertheless, Both networks show reasonable performance when the networks are very shallow. This further demonstrates that the performance of unfolded networks do not rely on a deep structure. For the structure simplicity and training speed, we set the number of iteration blocks as 1 for proposed method in the following experiments.

3) *Impact of Training Size:* In this experiment, we will evaluate the impact of training size on the unmixing performance of unfolding based learning algorithms. The same as before, we use a noisy synthetic HSI data with  $SNR = 25$ . The size of training dataset changes from 256 to 4096. The final results of SAD and RMSE are shown in Fig. 20. The same as abundance estimation case, when the size of training dataset is very small, the proposed U-ADMM-BUNet-II can achieve almost twice better SAD compared with MNN-BU. Both methods achieve similar performance when training size is big enough. It is noticeable that when size of training dataset increases from 256 to 512, the RMSE of U-ADMM-BUNet-

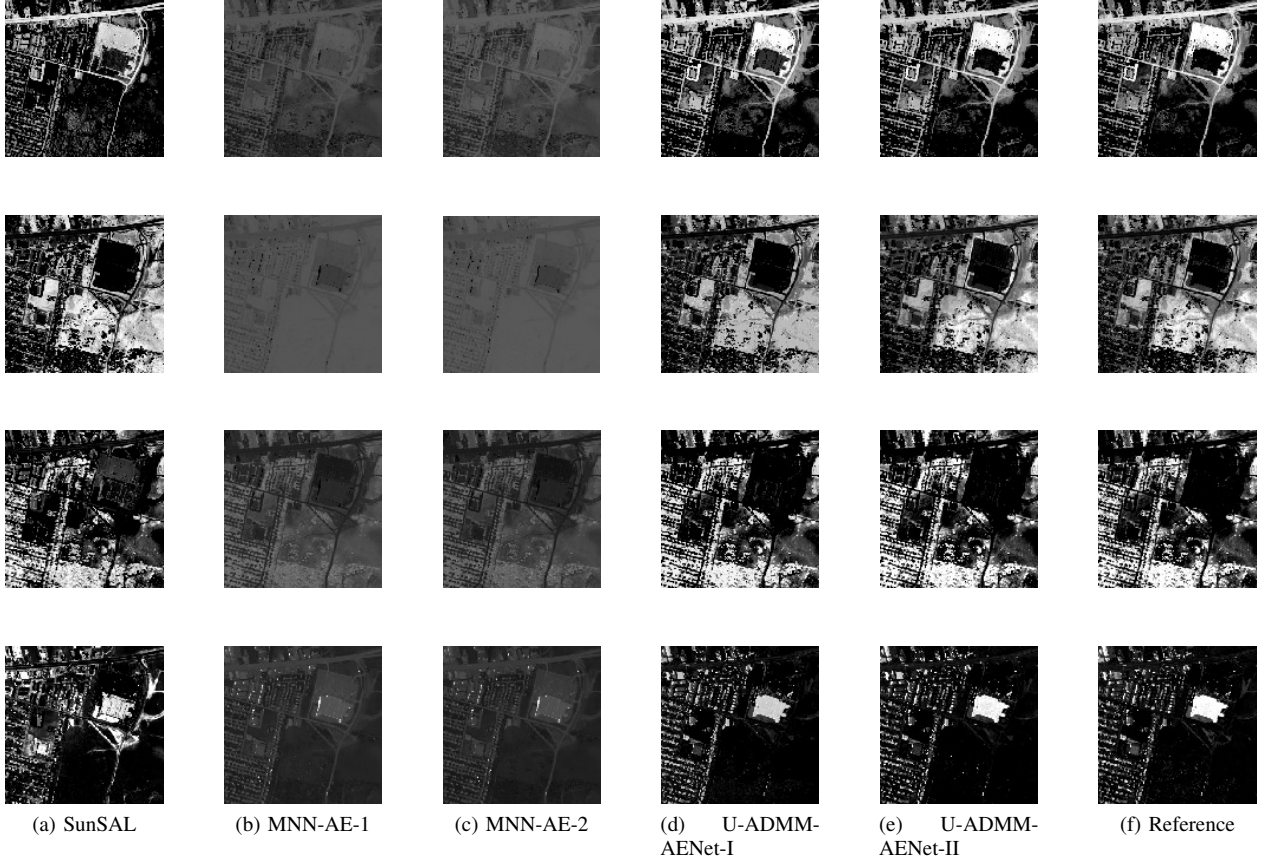


Fig. 17. Results of abundance estimation by different methods on Urban dataset. From top to bottom: Asphalt, Grass, Tree, and roof. (a) SunSAL. (b) MNN-AE-1. (c) MNN-AE-2. (d) U-ADMM-AENet-I. (e) U-ADMM-AENet-II. (f) Reference.

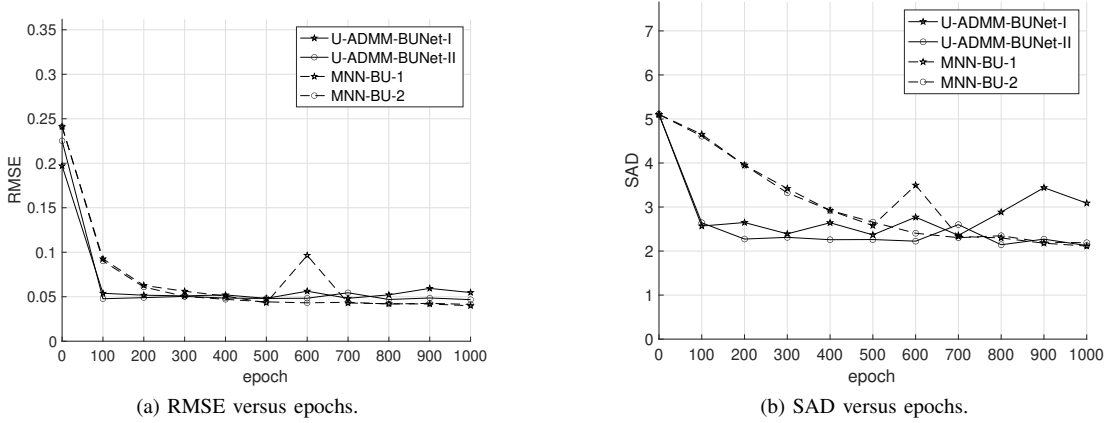


Fig. 18. The impact of training epochs on the performance of blind unmixing. (a) RMSE. (b) SAD in degree.

II increases. This may be the fact that RMSE depends on individual pixels, whereas endmember extraction depends on all training pixels.

4) *Impact of Noise*: In this experiment, we illustrate the impact of noise on the unmixing performance of all unmixing methods. For uDAS, MNN-BU-2 and proposed method, All the synthetic data are used for training and the final metrics are also evaluated on all synthetic pixels. For MVNTF, we use the default settings introduced in the original paper. The synthetic dataset are contaminated with different level of AWGN noise,

leading to  $SNR = [15, 20, 25, 30, inf]$ . It can be seen from Fig. 21 that, the proposed U-ADMM-BUNet-II achieves the best SAD when compared with other methods. In terms of RMSE, all learning based algorithms show a similar performance. Commonly, the learning based algorithms, uDAS, MNN-BU-2 and U-ADMM-BUNet-II, outperform the traditional nonnegative matrix factorization algorithms, MVNTF.



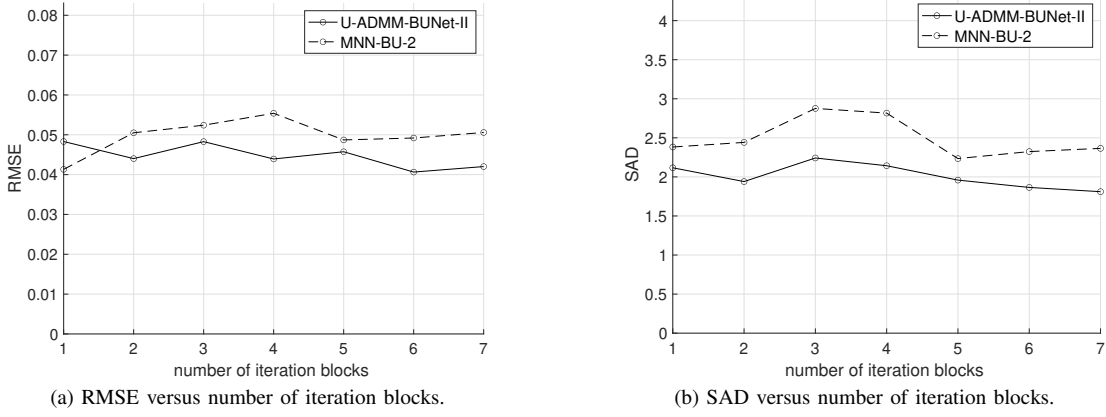


Fig. 19. The impact of number of iteration blocks on the performance of blind unmixing. (a) RMSE. (b) SAD in degree.

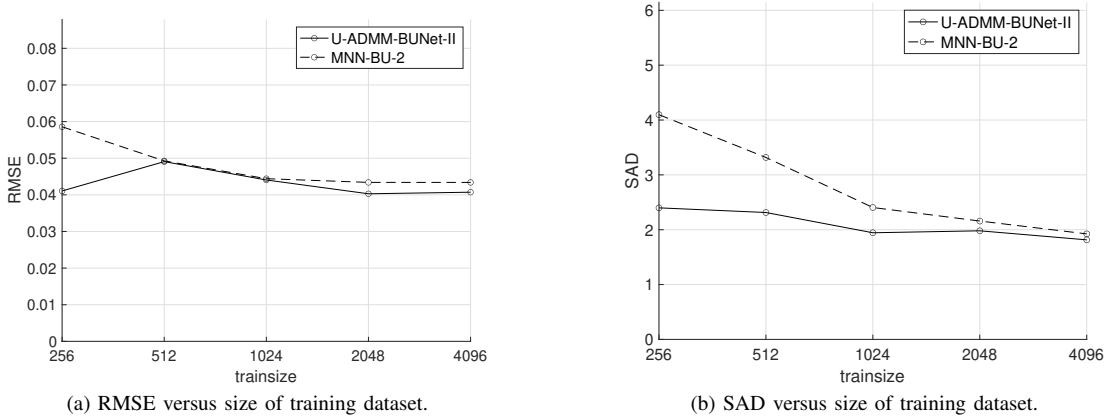


Fig. 20. The impact of size of training dataset on the performance of blind unmixing. (a) RMSE. (b) SAD in degree.

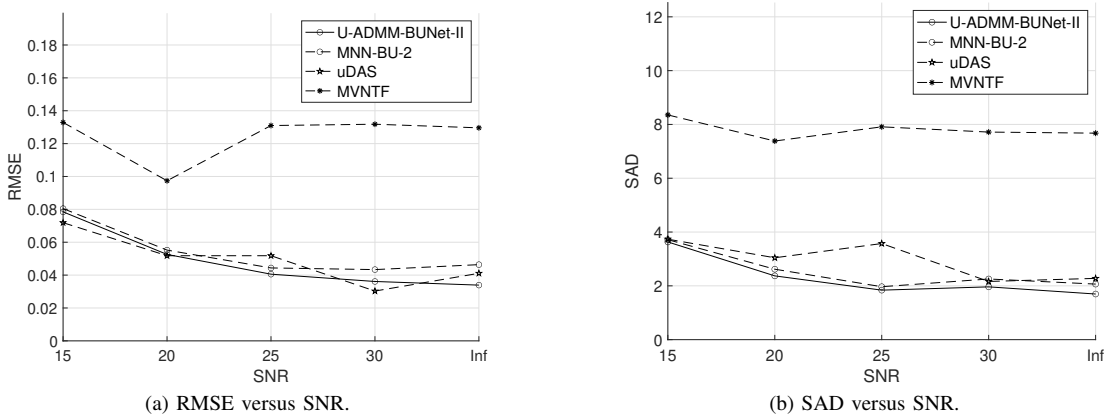


Fig. 21. The impact of SNR on the performance of blind unmixing. (a) RMSE. (b) SAD in degree.

### E. Blind Unmixing Comparison Using Real Hyperspectral Dataset

In this subsection, We compare the proposed U-ADMM-BUNet-II with competitors in real hyperspectral dataset. In short, we adopt the well-known Jasper Ridge [43], and Urban [44],[45], dataset for HSI unmixing. For learning based algorithms uDAS, MNN-BU-2 and the proposed U-ADMM-BUNet-II, we randomly choose 1000 pixels from the HSI

data as training pixels. All pixels are used for the evaluation of performance. All experiments are repeated five times. The mean and standard deviation are reported.

1) *Jasper Ridge*: The performance of various algorithms on Jasper Ridge dataset are shown in table II. Although the proposed U-ADMM-BUNet-II does not outperform the others in terms of individual endmember, it beats other in terms of average SAD performance. Another observation is that U-

TABLE II  
MEAN AND STANDARD DEVIATION OF SAD(IN DEGREES) BY DIFFERENT ALGORITHMS ON JASPER RIDGE AND URBAN. THE BEST RESULTS ARE IN BOLD.

Dataset	Endmember	uDAS	MV-NTF	MNN-BU-2	U-ADMM-BUNet-II
Jasper Ridge	Tree	10.0032±0.8436	15.3062±4.3640	<b>8.9695±0.4759</b>	10.2847±0.0423
	Water	7.6166±0.5672	15.1020±0.7648	<b>4.6415±0.2825</b>	5.1437±0.2528
	Soil	<b>6.6608±0.1950</b>	19.0967±13.5871	9.3849±1.0763	6.8969±0.0271
	Road	3.6029±0.1044	27.3426±2.7321	<b>3.3149±0.2417</b>	3.7676±0.0082
	Mean	6.9709±0.2659	19.2119±1.9248	6.5777±0.3295	<b>6.5232±0.0555</b>
Urban	Asphalt	12.3003± 0.1118	13.5129± 1.0604	11.0758± 0.1021	<b>10.4616± 0.0001</b>
	Grass	63.6797± 3.8035	19.3200± 3.9887	10.9092± 0.6905	<b>8.1522± 0.0003</b>
	Tree	7.6825± 1.2857	7.8657± 0.3075	<b>7.6598± 0.4615</b>	9.5990± 0.0002
	Roof	14.4911± 3.0348	27.7510± 2.6030	13.2186± 1.2686	<b>12.3660± 0.0004</b>
	Mean	24.5384± 2.0074	17.1124± 1.4393	10.7158± 0.3509	<b>10.1447± 0.0002</b>

ADMM-BUNet-II shows very stable performance as it has the lowest standard deviation. Fig. 22 illustrates the unscaled endmember signature estimation in dot line and corresponding true value in solid line. It can be seen from Fig. 23 that the proposed method also achieve a competitive performance compared to state-of-art methods.

2) *Urban*: The mean and standard deviation of SAD in degrees by various algorithms are shown in table II, where the best is in bold. It is clear that the proposed U-ADMM-BUNet-II outperforms other methods for Asphalt, Grass and Roof. Although MNN-BU-2 has the best estimation in terms of Tree, the proposed U-ADMM-BUNet-II achieves the best mean SAD among the competitors. Surprisingly, uDAS does not outperform MV-NTF in this dataset, which is mainly caused by the wrong estimation of Grass. This can be seen from Fig. 24, which illustrates the unscaled endmember signatures estimation in dot line and corresponding reference in solid line. The corresponding abundance maps are shown in Fig. 25.

## V. CONCLUSION

In this paper, we propose to construct hyperspectral unmixing network by unfolding a traditional optimization technique ADMM under a predefined linear mixture model. Through unfolding ADMM, we reformulate each iterative updating expression by replacing the fixed parameters with learnable parameters, which together, form a learnable neural network. We also show that the structure of each layer in the network unfolded from ADMM can find corresponding interpretation in machine learning literature, which further demonstrates the effectiveness of the proposed methods. This novel network structure combines the advantages of model based unmixing algorithms and learning based unmixing algorithms, providing a network with good interpretability and strong learning capacity. Compared with traditional iterative methods, the proposed methods can achieve fast unmixing as no iteration is needed once the network is trained. Compared with traditional

learning methods, the proposed network structures have much stronger interpretability. Based on this interpretability, we also propose two novel parameter initialization strategies, which can better incorporate the prior information to boost the performance of the network. Compared to existing unfolding based unmixing networks, the proposed network has a completely different structure, which possess both skipping connections and residual blocks, both of which have been shown powerful network structure in image processing field. In addition, to better fit in the unmixing problem, we propose to use a weighted loss between dissimilarity measurements from different perspectives. The novel network structure and training strategies allows the proposed network to achieve much faster convergence and reduce the reliance on a big training dataset. Both are very important in real hyperspectral application. Based on the LMM and autoencoder structure, we also propose unmixing network for blind unmixing by adding a linear layer at the end of proposed network structures. Extensive experiments on both synthetic and real HSI data have demonstrate the effectiveness of proposed methods.

## REFERENCES

- [1] G. Shaw and D. Manolakis, "Signal processing for hyperspectral image exploitation," *IEEE Signal Processing Magazine*, vol. 19, no. 1, pp. 12–16, 2002.
- [2] N. Keshava and J. F. Mustard, "Spectral unmixing," *IEEE Signal Processing Magazine*, vol. 19, no. 1, pp. 44–57, 2002.
- [3] G. Camps-Valls, D. Tuia, L. Gmez-Chova, and S. Jimnez, *Remote Sensing Image Processing*. Morgan and Claypool, 2011. [Online]. Available: <https://ieeexplore.ieee.org/document/6813744>
- [4] J. M. P. Nascimento and J. M. B. Dias, "Vertex component analysis: a fast algorithm to unmix hyperspectral data," *IEEE Transactions on Geoscience and Remote Sensing*, vol. 43, no. 4, pp. 898–910, 2005.
- [5] C. . Chang, C. . Wu, W. Liu, and Y. . Ouyang, "A new growing method for simplex-based endmember extraction algorithm," *IEEE Transactions on Geoscience and Remote Sensing*, vol. 44, no. 10, pp. 2804–2819, 2006.
- [6] T. Chan, W. Ma, A. Ambikapathi, and C. Chi, "A simplex volume maximization framework for hyperspectral endmember extraction," *IEEE Transactions on Geoscience and Remote Sensing*, vol. 49, no. 11, pp. 4177–4193, 2011.

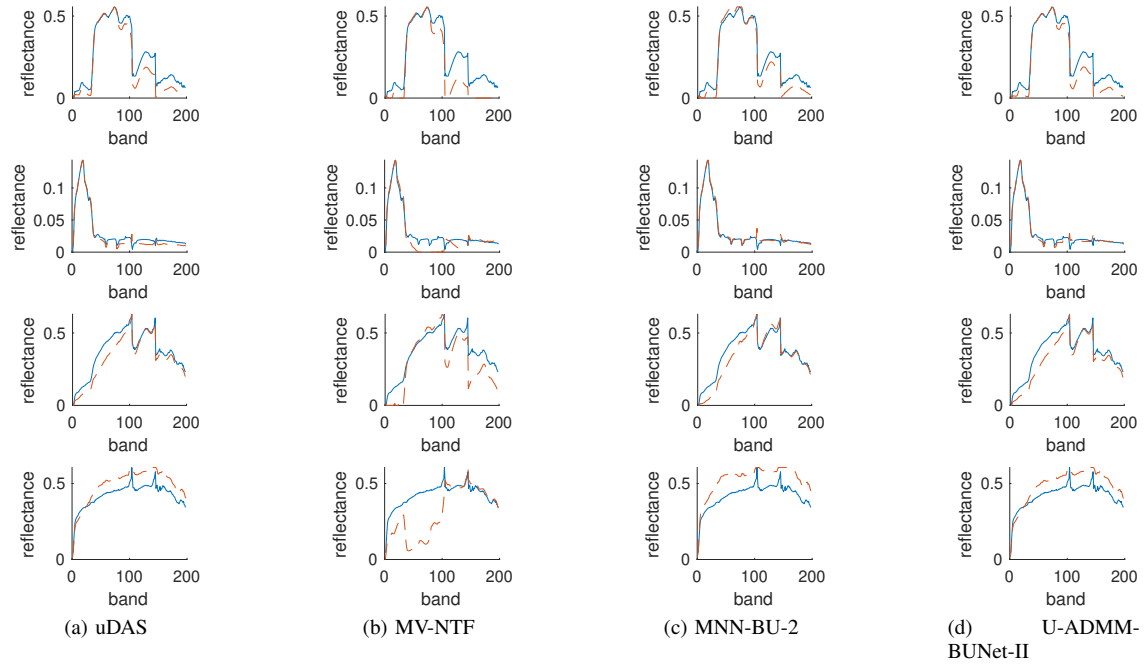


Fig. 22. Estimated endmember signatures of blind unmixing by different methods on Jasper Ridge dataset. Solid line indicates the true value, while dot line indicates the scaled estimated value. From top to bottom: Tree, Water, Soil, and Road. (a) uDAS. (b) MV-NTF. (c) MNN-BU-2. (d) U-ADMM-BUNet-II.

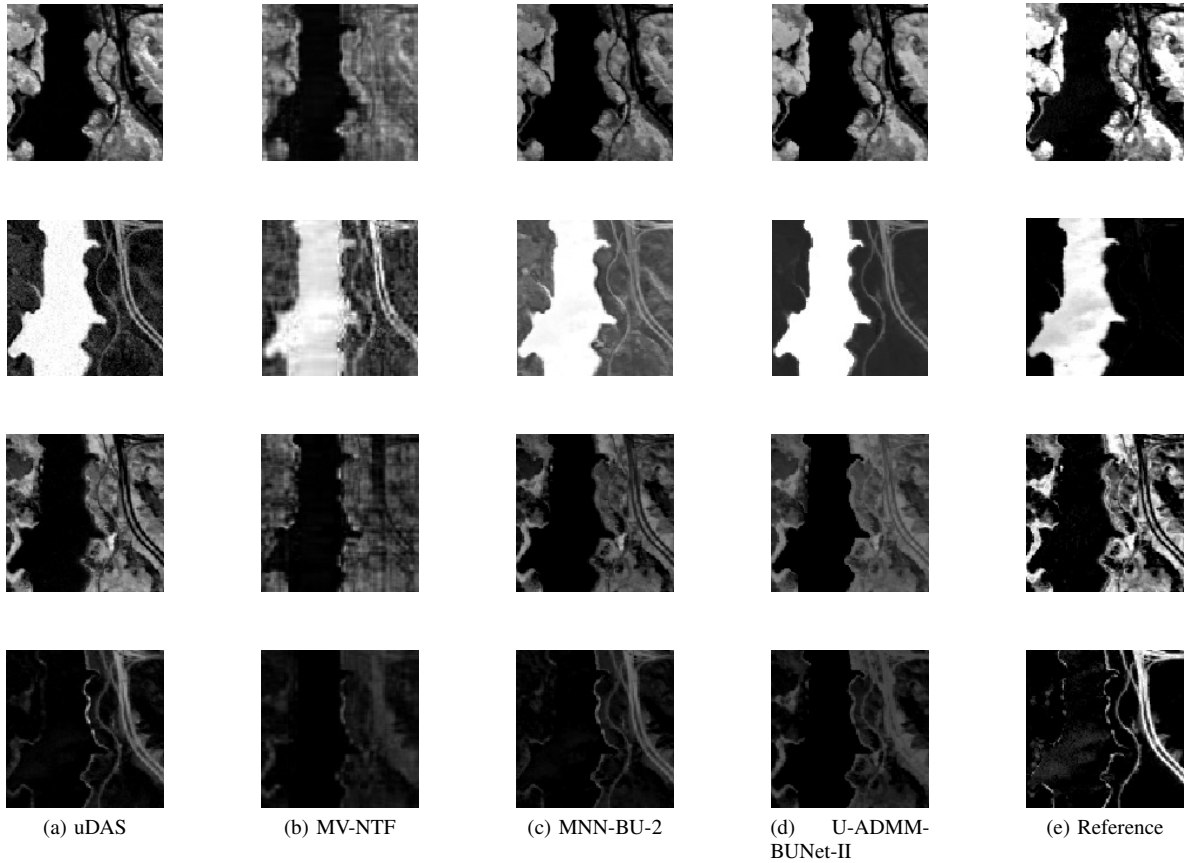


Fig. 23. Estimated abundance map of blind unmixing by different methods on Jasper Ridge dataset. From top to bottom: Tree, Water, Soil, and Road. (a) uDAS. (b) MV-NTF. (c) MNN-BU-2. (d) U-ADMM-BUNet-II. (e) Reference.

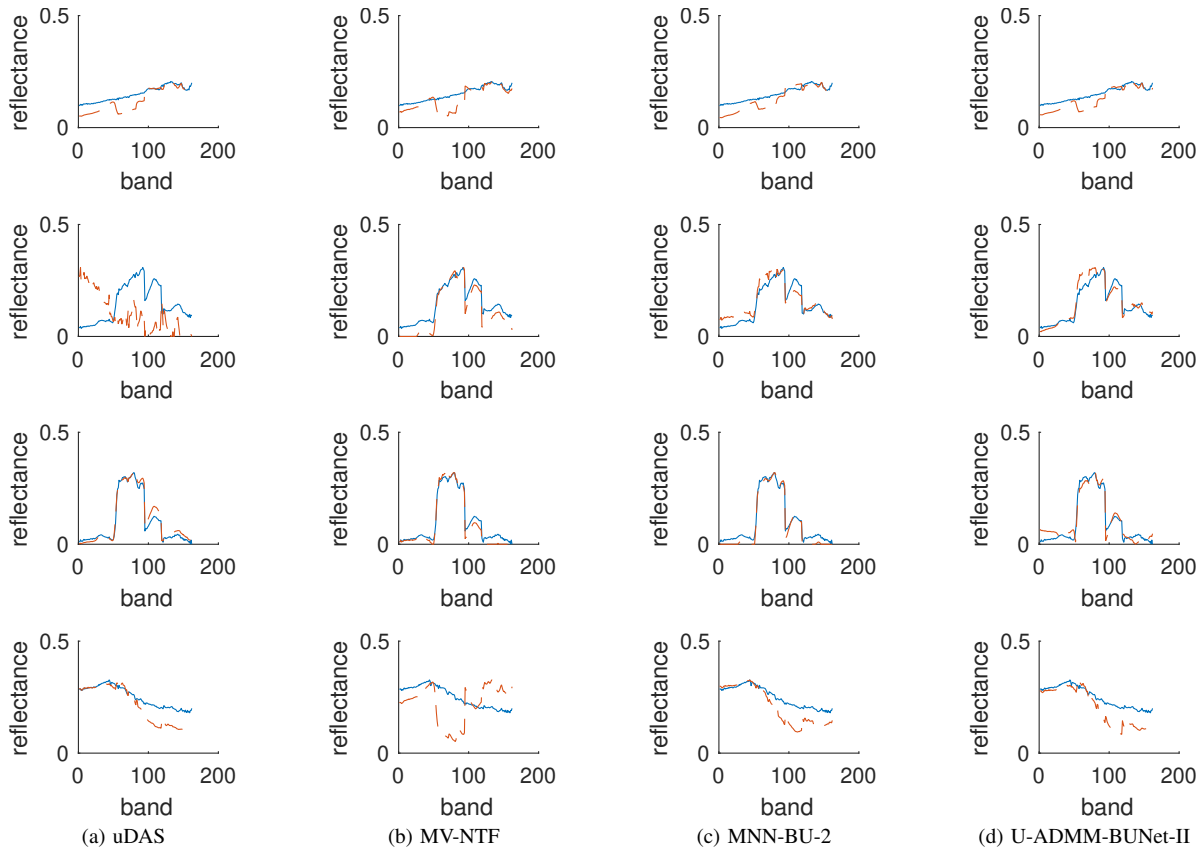


Fig. 24. Estimated endmember signatures of blind unmixing by different methods on Urban dataset. Solid line indicates the true value, while dot line indicates the scaled estimated value. From top to bottom: Asphalt, Grass, Tree, and roof. (a) uDAS. (b) MV-NTF. (c) MNN-BU-2. (d) U-ADMM-BUNet-II.

- [8] J. M. P. Nascimento and J. M. Bioucas-Dias, "Hyperspectral unmixing based on mixtures of dirichlet components," *IEEE Transactions on Geoscience and Remote Sensing*, vol. 50, no. 3, pp. 863–878, 2012.
- [9] A. M. Bruckstein, M. Elad, and M. Zibulevsky, "Sparse non-negative solution of a linear system of equations is unique," in *2008 3rd International Symposium on Communications, Control and Signal Processing*, 2008, pp. 762–767.
- [10] Y. C. Pati, R. Rezaeiifar, and P. S. Krishnaprasad, "Orthogonal matching pursuit: recursive function approximation with applications to wavelet decomposition," in *Proceedings of 27th Asilomar Conference on Signals, Systems and Computers*, 1993, pp. 40–44 vol.1.
- [11] M. Iordache, J. M. Bioucas-Dias, and A. Plaza, "Sparse unmixing of hyperspectral data," *IEEE Transactions on Geoscience and Remote Sensing*, vol. 49, no. 6, pp. 2014–2039, 2011.
- [12] J. M. Bioucas-Dias and M. A. T. Figueiredo, "Alternating direction algorithms for constrained sparse regression: Application to hyperspectral unmixing," in *2010 2nd Workshop on Hyperspectral Image and Signal Processing: Evolution in Remote Sensing*, 2010, pp. 1–4.
- [13] M. Iordache, J. M. Bioucas-Dias, and A. Plaza, "Collaborative sparse regression for hyperspectral unmixing," *IEEE Transactions on Geoscience and Remote Sensing*, vol. 52, no. 1, pp. 341–354, 2014.
- [14] G. A. Licciardi and F. Del Frate, "Pixel unmixing in hyperspectral data by means of neural networks," *IEEE Transactions on Geoscience and Remote Sensing*, vol. 49, no. 11, pp. 4163–4172, 2011.
- [15] F. Palsson, J. Sigurdsson, J. R. Sveinsson, and M. O. Ulfarsson, "Neural network hyperspectral unmixing with spectral information divergence objective," in *2017 IEEE International Geoscience and Remote Sensing Symposium (IGARSS)*, 2017, pp. 755–758.
- [16] B. Palsson, J. Sigurdsson, J. R. Sveinsson, and M. O. Ulfarsson, "Hyperspectral unmixing using a neural network autoencoder," *IEEE Access*, vol. 6, pp. 25 646–25 656, 2018.
- [17] S. Özkan and G. B. Akar, "Improved deep spectral convolution network for hyperspectral unmixing with multinomial mixture kernel and endmember uncertainty," *CoRR*, vol. abs/1808.01104, 2018. [Online]. Available: <http://arxiv.org/abs/1808.01104>
- [18] Y. Su, J. Li, A. Plaza, A. Marinoni, P. Gamba, and S. Chakravorty, "Daen: Deep autoencoder networks for hyperspectral unmixing," *IEEE Transactions on Geoscience and Remote Sensing*, vol. 57, no. 7, pp. 4309–4321, 2019.
- [19] K. Gregor and Y. LeCun, "Learning fast approximations of sparse coding," in *Proceedings of the 27th International Conference on International Conference on Machine Learning*, ser. ICML10. Madison, WI, USA: Omnipress, 2010, p. 399406.
- [20] X. Deng and P. L. Dragotti, "Deep convolutional neural network for multi-modal image restoration and fusion," 2019.
- [21] Q. Qian, F. Xiong, and J. Zhou, "Deep unfolded iterative shrinkage-thresholding model for hyperspectral unmixing," in *IGARSS 2019 - 2019 IEEE International Geoscience and Remote Sensing Symposium*, 2019, pp. 2151–2154.
- [22] J. M. Bioucas-Dias, A. Plaza, G. Camps-Valls, P. Scheunders, N. Nasrabadi, and J. Chanussot, "Hyperspectral remote sensing data analysis and future challenges," *IEEE Geoscience and Remote Sensing Magazine*, vol. 1, no. 2, pp. 6–36, 2013.
- [23] H. Lee, A. Battle, R. Raina, and A. Y. Ng, "Efficient sparse coding algorithms," in *Proceedings of the 19th International Conference on Neural Information Processing Systems*, ser. NIPS06. Cambridge, MA, USA: MIT Press, 2006, p. 801808.
- [24] U. S. Kamilov and H. Mansour, "Learning optimal nonlinearities for iterative thresholding algorithms," *IEEE Signal Processing Letters*, vol. 23, no. 5, pp. 747–751, 2016.
- [25] J. M. Bioucas-Dias and M. A. T. Figueiredo, "Alternating direction algorithms for constrained sparse regression: Application to hyperspectral unmixing," in *2010 2nd Workshop on Hyperspectral Image and Signal Processing: Evolution in Remote Sensing*, 2010, pp. 1–4.
- [26] S. Boyd, N. Parikh, E. Chu, B. Peleato, and J. Eckstein, "Distributed optimization and statistical learning via the alternating direction method of multipliers," *Found. Trends Mach. Learn.*, vol. 3, no. 1, p. 1122, Jan. 2011. [Online]. Available: <https://doi.org/10.1561/22000000016>
- [27] I. Daubechies, M. Defrise, and C. De Mol, "An iterative thresholding algorithm for linear inverse problems with a sparsity constraint," *Com-*

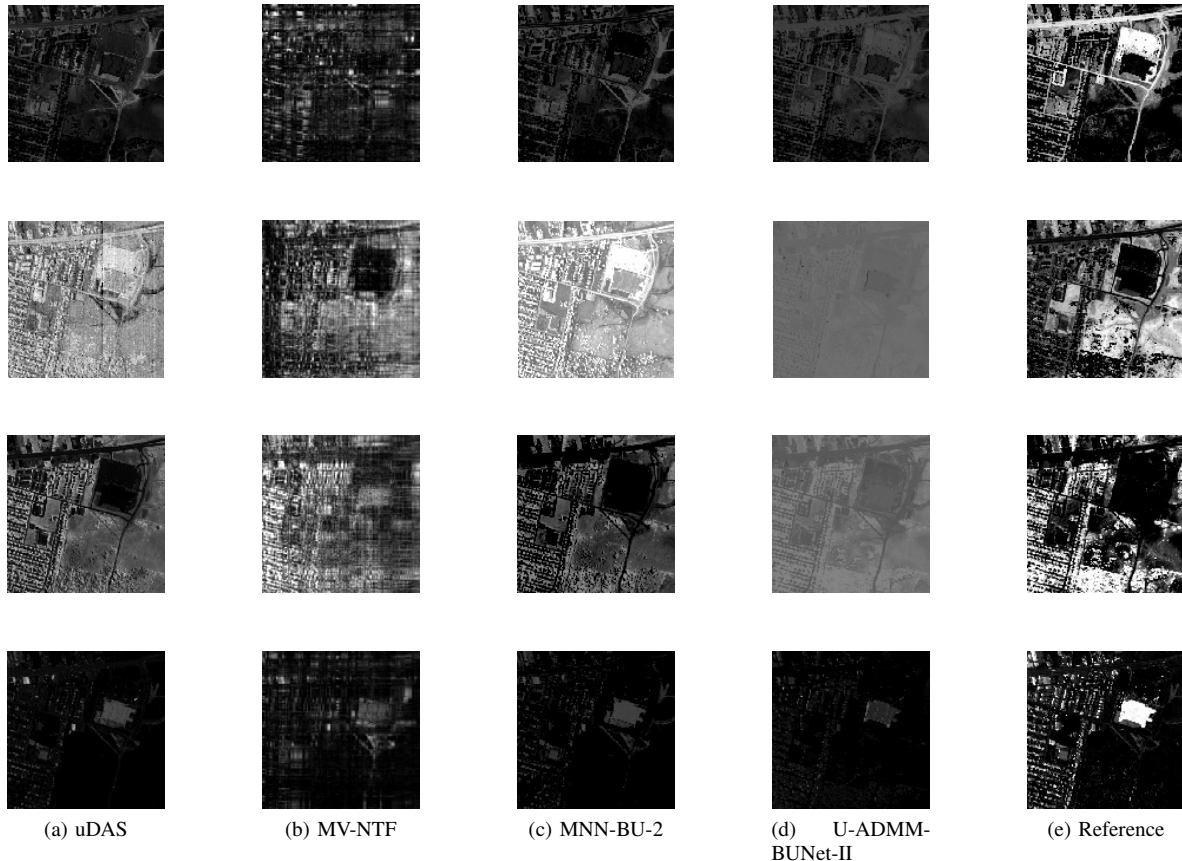


Fig. 25. Estimated abundance map of blind unmixing by different methods on Urban dataset. From top to bottom: Asphalt, Grass, Tree, and roof. (a) uDAS. (b) MV-NTF. (c) MNN-BU-2. (d) U-ADMM-BUNet-II. (e) Reference.

- munications on Pure and Applied Mathematics*, vol. 57, no. 11, pp. 1413–1457, 2004.
- [28] D. D. Lee and H. S. Seung, “Algorithms for non-negative matrix factorization,” in *Proceedings of the 13th International Conference on Neural Information Processing Systems*, ser. NIPS00. Cambridge, MA, USA: MIT Press, 2000, p. 535541.
- [29] X. Zhang, Y. Sun, J. Zhang, P. Wu, and L. Jiao, “Hyperspectral unmixing via deep convolutional neural networks,” *IEEE Geoscience and Remote Sensing Letters*, vol. 15, no. 11, pp. 1755–1759, 2018.
- [30] C. Szegedy, Wei Liu, Yangqing Jia, P. Sermanet, S. Reed, D. Anguelov, D. Erhan, V. Vanhoucke, and A. Rabinovich, “Going deeper with convolutions,” in *2015 IEEE Conference on Computer Vision and Pattern Recognition (CVPR)*, 2015, pp. 1–9.
- [31] Y. Qu and H. Qi, “udas: An untied denoising autoencoder with sparsity for spectral unmixing,” *IEEE Transactions on Geoscience and Remote Sensing*, vol. 57, no. 3, pp. 1698–1712, 2019.
- [32] R. A. Borsoi, T. Imbiriba, and J. C. M. Bermudez, “Deep generative endmember modeling: An application to unsupervised spectral unmixing,” *IEEE Transactions on Computational Imaging*, vol. 6, pp. 374–384, 2020.
- [33] S. Ozkan, B. Kaya, and G. B. Akar, “Endnet: Sparse autoencoder network for endmember extraction and hyperspectral unmixing,” *IEEE Transactions on Geoscience and Remote Sensing*, vol. 57, no. 1, pp. 482–496, 2019.
- [34] I. Marivani, E. Tsiligianni, B. Cornelis, and N. Deligiannis, “Multimodal image super-resolution via deep unfolding with side information,” in *2019 27th European Signal Processing Conference (EUSIPCO)*, 2019, pp. 1–5.
- [35] Y. Qian, F. Xiong, Q. Qian, and J. Zhou, “Spectral mixture model inspired network architectures for hyperspectral unmixing,” *IEEE Transactions on Geoscience and Remote Sensing*, pp. 1–17, 2020.
- [36] K. He, X. Zhang, S. Ren, and J. Sun, “Deep residual learning for image recognition,” in *2016 IEEE Conference on Computer Vision and Pattern Recognition (CVPR)*, 2016, pp. 770–778.
- [37] B. Lim, S. Son, H. Kim, S. Nah, and K. M. Lee, “Enhanced deep residual networks for single image super-resolution,” in *2017 IEEE Conference on Computer Vision and Pattern Recognition Workshops (CVPRW)*, 2017, pp. 1132–1140.
- [38] K. Zhang, W. Zuo, Y. Chen, D. Meng, and L. Zhang, “Beyond a gaussian denoiser: Residual learning of deep cnn for image denoising,” *IEEE Transactions on Image Processing*, vol. 26, no. 7, pp. 3142–3155, 2017.
- [39] J. Kim, J. K. Lee, and K. M. Lee, “Accurate image super-resolution using very deep convolutional networks,” in *2016 IEEE Conference on Computer Vision and Pattern Recognition (CVPR)*, 2016, pp. 1646–1654.
- [40] W. Lai, J. Huang, N. Ahuja, and M. Yang, “Deep laplacian pyramid networks for fast and accurate super-resolution,” in *2017 IEEE Conference on Computer Vision and Pattern Recognition (CVPR)*, 2017, pp. 5835–5843.
- [41] S. Jia and Y. Qian, “Constrained nonnegative matrix factorization for hyperspectral unmixing,” *IEEE Transactions on Geoscience and Remote Sensing*, vol. 47, no. 1, pp. 161–173, 2009.
- [42] “Usgs library,” <https://www.usgs.gov/labs/spec-lab>.
- [43] F. Zhu, Y. Wang, S. Xiang, B. Fan, and C. Pan, “Structured Sparse Method for Hyperspectral Unmixing,” *ISPRS Journal of Photogrammetry and Remote Sensing*, vol. 88, pp. 101–118, 2014. [Online]. Available: <http://www.sciencedirect.com/science/article/pii/S0924271613002761>
- [44] Y. Qian, S. Jia, J. Zhou, and A. Robles-Kelly, “Hyperspectral unmixing via  $l_{1/2}$  sparsity-constrained nonnegative matrix factorization,” *IEEE Transactions on Geoscience and Remote Sensing*, vol. 49, no. 11, pp. 4282–4297, 2011.
- [45] F. Zhu, Y. Wang, B. Fan, S. Xiang, G. Meng, and C. Pan, “Spectral unmixing via data-guided sparsity,” *IEEE Transactions on Image Processing*, vol. 23, no. 12, pp. 5412–5427, 2014.
- [46] Y. Qian, F. Xiong, S. Zeng, J. Zhou, and Y. Y. Tang, “Matrix-vector nonnegative tensor factorization for blind unmixing of hyperspectral imagery,” *IEEE Transactions on Geoscience and Remote Sensing*, vol. 55, no. 3, pp. 1776–1792, 2017.